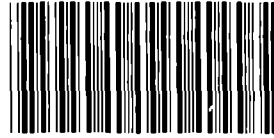


SANDIA REPORT

SAND92-0347 • UC-910

Unlimited Release

Printed May 1993



#8569565*

MICROFILM
SERIALS
SECTION
UNIVERSITY
OF CALIFORNIA
LIBRARY**SANDIA NATIONAL
LABORATORIES
TECHNICAL LIBRARY****Comparison of Analytic Whipple Bumper
Shield Ballistic Limits with CTH Simulations**

Eugene S. Hertel, Jr.

Prepared by
Sandia National Laboratories
Albuquerque, New Mexico 87185 and Livermore, California 94550
for the United States Department of Energy
under Contract DE-AC04-76DP00789

Issued by Sandia National Laboratories, operated for the United States Department of Energy by Sandia Corporation.

NOTICE: This report was prepared as an account of work sponsored by an agency of the United States Government. Neither the United States Government nor any agency thereof, nor any of their employees, nor any of their contractors, subcontractors, or their employees, makes any warranty, express or implied, or assumes any legal liability or responsibility for the accuracy, completeness, or usefulness of any information, apparatus, product, or process disclosed, or represents that its use would not infringe privately owned rights. Reference herein to any specific commercial product, process, or service by trade name, trademark, manufacturer, or otherwise, does not necessarily constitute or imply its endorsement, recommendation, or favoring by the United States Government, any agency thereof or any of their contractors or subcontractors. The views and opinions expressed herein do not necessarily state or reflect those of the United States Government, any agency thereof or any of their contractors.

Printed in the United States of America. This report has been reproduced directly from the best available copy.

Available to DOE and DOE contractors from
Office of Scientific and Technical Information
PO Box 62
Oak Ridge, TN 37831

Prices available from (615) 576-8401, FTS 626-8401

Available to the public from
National Technical Information Service
US Department of Commerce
5285 Port Royal Rd
Springfield, VA 22161

NTIS price codes
Printed copy: A04
Microfiche copy: A01

Comparison of Analytic Whipple Bumper Shield Ballistic Limits with CTH Simulations

Eugene S. Hertel, Jr.
Computational Physics Research and Development Department
Sandia National Laboratories
Albuquerque, NM 87185

Abstract

A series of CTH simulations were conducted to assess the feasibility of using the hydrodynamic code for debris cloud formation and to predict any damage due to the subsequent loading on rear structures. Six axisymmetric and one 3-dimensional simulations were conducted for spherical projectiles impacting Whipple bumper shields. The projectile diameters were chosen to correlate with two well known analytic expressions for the ballistic limit of a Whipple bumper shield. It has been demonstrated that CTH can be used to simulate the debris cloud formation, the propagation of the debris across a void region, and the secondary impact of the debris against a structure. In addition, the results from the CTH simulations were compared to the analytic estimates of the ballistic limit. At impact velocities of 10 km/s or less, the CTH predicted ballistic limit lays between the two analytic estimates. However, for impact velocities greater than 10 km/s, CTH simulations predicted a ballistic limit larger than both analytical estimates. The differences at high velocities are not well understood. Structural failure at late times due to the time integrated loading of a very diffuse debris cloud has not been considered in the CTH model. In addition, the analytic predictions are extrapolated from relatively low velocity data and the extrapolation technique may not be valid. The discrepancy between the two techniques should be investigated further.

Acknowledgment

The author would like to acknowledge Dr. Pedro Rodriguez and Mr. Scott Hill for providing partial funding for these studies. In addition, Lane Yarrington and Mike McGlaun need to be acknowledged for their assistance with some of the calculations.

Comparison of Analytic Whipple Bumper Shield Ballistic Limits with CTH Simulations

Contents

Acknowledgment.....	4
Introduction.....	9
Analytic Ballistic Limit Curves.....	10
Bumper Shields as a Technique for Debris Protection.....	10
Wilkinson Ballistic Limit Curve.....	11
Cour-Palais Ballistic Limit Curve.....	12
Modified Cour-Palais Ballistic Limit Curve.....	13
CTH Simulations.....	15
CTH Overview.....	15
Computational Technique.....	17
CTH Results.....	20
Normal Impact.....	20
Oblique Impact.....	40
Conclusions.....	45
References.....	47
APPENDIX—Sample CTH Input Deck for Axis-Symmetric Simulation.....	49
APPENDIX—CTH Input Deck for Three-Dimensional Simulation.....	53
Acknowledgment.....	4

Tables

Table 1.	Projectile Parameters for the CTH Simulations.....	17
Table 2.	Initial X Zoning	18
Table 3.	Initial Y Zoning	18
Table 4.	Initial Z Zoning.....	19
Table 5.	Final X Zoning.....	19
Table 6.	Final Y Zoning.....	19
Table 7.	Final Z Zoning	19
Table 8.	Strength Parameters used for CTH Simulations.....	20
Table 9.	CTH Penetration Predictions for the Axisymmetric Simulations.....	21
Table 10.	CTH Estimates of the Thermodynamic State of the Debris Cloud.....	21

Figures

Figure 1. A Typical Whipple Bumper Shield	10
Figure 2. Conceptual Ballistic Limit for an Aluminum Whipple-like Bumper Shield	11
Figure 3. Wilkinson Ballistic Limit for a Whipple Bumper Shield	13
Figure 4. Cour-Palais Ballistic Limit for a Whipple Bumper Shield	14
Figure 5. Modified Cour-Palais Ballistic Limit for a Whipple Bumper Shield	16
Figure 6. A Comparison of Three Ballistic Limit Curves above 7 km/s	16
Figure 7. The na8-w CTH Simulation Halfway Between the Bumper and Rear Wall.....	22
Figure 8. The na8-w CTH Simulation Just Before Rear Wall Impact	23
Figure 9. The na8-w CTH Simulation Rear Wall Terminal Damage	24
Figure 10. The na8-mcp CTH Simulation Halfway Between the Bumper and Rear Wall	25
Figure 11. The na8-mcp CTH Simulation Just Before Rear Wall Impact	26
Figure 12. The na8-mcp CTH Simulation Rear Wall Terminal Damage	27
Figure 13. The na10-w CTH Simulation Halfway Between the Bumper and Rear Wall	28
Figure 14. The na10-w CTH Simulation Just Before Rear Wall Impact	29
Figure 15. The na10-w CTH Simulation Rear Wall Terminal Damage	30
Figure 16. The na10-mcp CTH Simulation Halfway Between the Bumper and Rear Wall	31
Figure 17. The na10-mcp CTH Simulation Just Before Rear Wall Impact	32
Figure 18. The na10-mcp CTH Simulation Rear Wall Terminal Damage	33
Figure 19. The na12-w CTH Simulation Halfway Between the Bumper and Rear Wall	34
Figure 20. The na12-w CTH Simulation Just Before the Rear Wall	35
Figure 21. The na12-w CTH Simulation Rear Wall Terminal Damage	36
Figure 22. The na12-mcp CTH Simulation Halfway Between the Bumper and Rear Wall	37
Figure 23. The na12-mcp CTH Simulation Just Before the Rear Wall	38
Figure 24. The na12-mcp CTH Simulation Rear Wall Terminal Damage	39
Figure 25. Computational Radiograph of CTH Simulation na12-ob at 2 μ s	40
Figure 26. 3D Perspective View of CTH Simulation na12-ob at 2 μ s.....	41
Figure 27. Computational Radiograph of CTH Simulation na12-ob at 11 μ s	42
Figure 28. 3D Perspective View of CTH Simulation na12-ob at 11 μ s.....	43
Figure 29. Terminal Rear Wall Damage for CTH Simulation na12-ob at 21 μ s	44
Figure 30. A Comparison of CTH and Analytic Ballistic Limits	45

Comparison of Analytic Whipple Bumper Shield Ballistic Limits with CTH Simulations

Introduction

It is well known that the principal threat to orbiting space structures results from impact damage caused by orbiting space debris. Presently, laboratory facilities are only just becoming available^{1,2,3} for evaluating damage mechanisms or the effectiveness of protective structures against this debris. In light of such capabilities, analytic methods^{4,5,6} for predicting impact damage have been used extensively to date. These analytic techniques generally consist of a fit-to-data at experimentally assessable velocities (to date, at velocities less than ~ 7.5 km/s) coupled with an extrapolation to higher velocities. The extrapolations are generally based on energy or momentum partitioning. Hydrodynamics code simulations⁷ of impact events are also used to estimate impact damage. Both of these techniques have progressed to the point of providing realistic damage assessments, although, these analyses or models have not been validated at velocities in excess of ~ 7.5 km/s. Experimental results evaluating various Whipple bumper shields are just becoming available and are expected to be useful in refining similar analyses.

A requirement for an effective debris shield is that it must protect the spacecraft from impacts both from the micrometeoroid and orbital debris environment. The micrometeoroid environment is thought to result from dust-size particles having an average velocity of 20 km/s, while the orbital debris environment is believed to be millimeter or centimeter size particles weighing approximately a gram with average velocities of 10 km/s. It is generally assumed that the average density of the orbital debris environment is ~ 2.8 gm/cm³, and therefore can be represented by the material properties of aluminum. The orbital debris environment, which is man-made space debris is more hazardous than the micrometeoroid environment because of its relatively large mass and particle size. This makes the design requirements for an adequate bumper shield difficult to establish. This also places the critical portion the velocity spectrum in a region outside of conventional experimental techniques to date. It is in this region that a comparison between the analytic and hydrodynamics code damage predictions has been made.

The next section will give the background of debris shielding and describe the analytic damage prediction curves that are in use today. The following section will describe the CTH hydrodynamics code and give the results of the simulations. The final section will discuss the comparison of the two methods.

Analytic Ballistic Limit Curves

Bumper Shields as a Technique for Debris Protection

The bumper shield concept originally proposed by Whipple⁸ remains the basis for all simple shielding designs under consideration today. The Whipple bumper shield concept consists of a relatively thin sheet of material that is spaced some distance from the protected component, usually a thicker rear wall. In theory, incoming projectile impacts the bumper and are fragmented and dispersed. The protected component must then withstand encounters with a debris cloud formed from bumper material and the original projectile. Figure 1 shows a schematic of a typical Whipple bumper shield. In theory, the protected

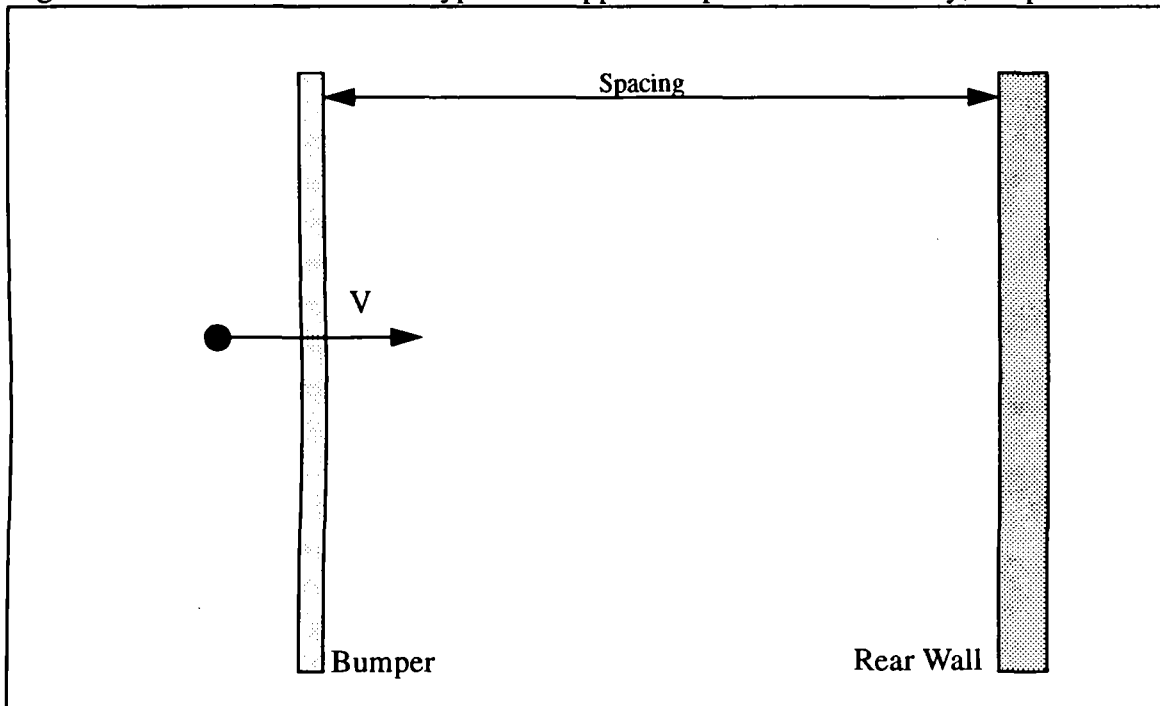


Figure 1. A Typical Whipple Bumper Shield

component can be lightened to offset the additional mass of the bumper structure without sacrificing the overall impact resistance.

It was realized⁹ that a number of variables control the effectiveness of such a shield. The typical variables considered are the size and velocity of the incoming projectile, the bumper and rear wall thickness, the bumper and rear wall material, and the bumper to rear wall spacing. The concept of effectiveness is usually described by a ballistic limit curve. The ballistic limit curve for a particular bumper shield design is given in terms of a critical diameter of an impacting projectile. The critical diameter of the impacting projectile is that diameter that just perforates the rear wall. Some organizations chose to include other damage criteria, such as detached spall, in defining "perforation." The ballistic limit curve is defined as the locus of points in critical diameter-velocity space such that any projectile

(at a given velocity) greater in size than predicted by the curve would penetrate the rear wall. A hypothetical ballistic limit curve is shown in Figure 2.

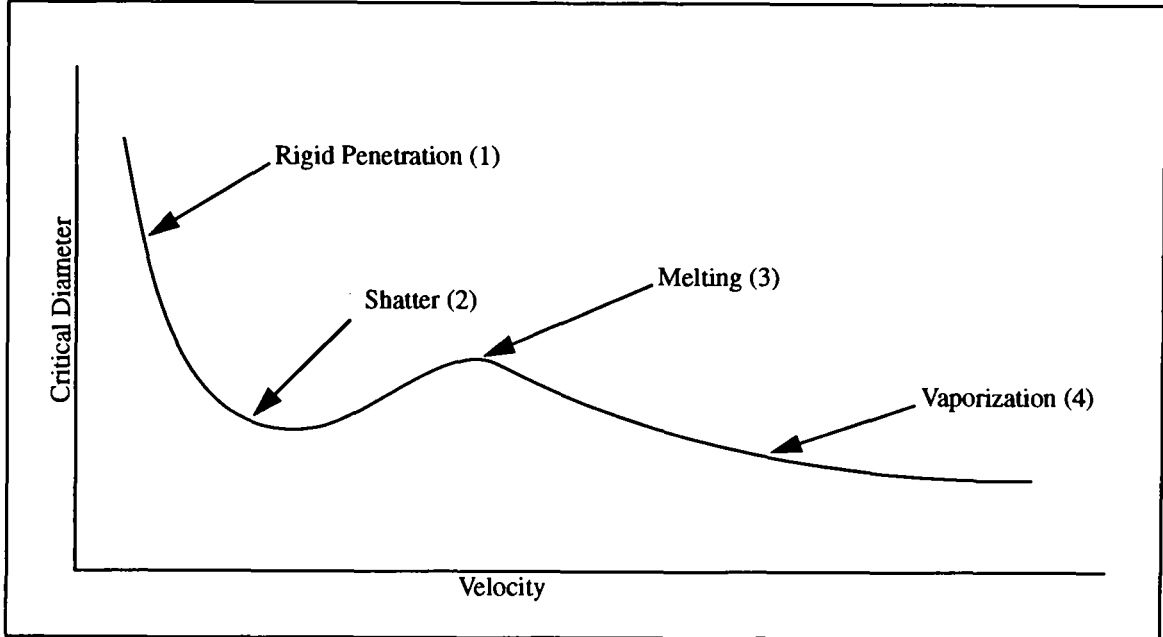


Figure 2. Conceptual Ballistic Limit for an Aluminum Whipple-like Bumper Shield

The regions of the curve in Figure 2 are interesting to illustrate the various thermodynamic phase changes that take place in aluminum-on-aluminum impacts. The first region (1) is that of rigid penetration, at low velocity, the bumper is perforated by the projectile and the rear wall provides most of the stopping power of the shield system. As the velocity increases, the critical diameter decreases as the energy increases. At some point (2), the incoming projectile starts to fragment and disperse. The critical diameter will then increase as the individual fragment size becomes the controlling factor in rear wall penetration. Between impact velocities of 5.7 and 6.9 km/s, a transition from incipient to complete melt occurs. Near point 3, even though the debris cloud is composed of molten droplets, the energy increases so that the critical diameter will decrease. At velocities above 10.4 km/s (4), the debris cloud should start to vaporize. Even though vaporization starts at ~10 km/s, some condensed phased material will be present in the debris cloud for very high impact velocities. It may be the effect of this residual condensed material that accounts for the relatively low critical diameter at very high impact velocities.

The current analytic ballistic limit curves will be discussed in the following sections. The disagreement between the analytic curves is centered in the velocity regime above 8 km/s which are above experimentally assessable impact velocities.

Wilkinson Ballistic Limit Curve

The Wilkinson⁴ equation was formulated almost entirely from analytical considerations, with relatively little correlation with experimental data. This method relies on classical fragmentation and penetration theory to develop the debris cloud and predict rear wall

Comparison of Analytic Whipple Bumper Shield Ballistic Limits with CTH Simulations

perforation. Rearranging the equations from Reference 4 to yield an expression in terms of critical diameter gives:

$$d_c = 1.2878 \left((KC_s) (t_b t_r) \left((\rho_b \rho_r) / V \right) \right)^{1/4} \sqrt{S} / \sqrt{\rho}. \quad (1)$$

The terms are defined as

- d_c critical diameter (cm)
- K constant depending on rear wall material (~0.6)
- C_s sound speed of rear wall material (km/s)
- t_b bumper thickness (cm)
- t_r rear wall thickness (cm)
- ρ_b bumper density (gm/cm³)
- ρ_r rear wall density (gm/cm³)
- V projectile velocity (km/s)
- S bumper-rear wall spacing (cm)
- ρ projectile density (gm/cm³).

In the original publication, this curve is used throughout the velocity spectrum. At this time, a curve fit to the experimental database is used for velocities below ~7 km/s. The next section will describe the fit to experimental data. Figure 3 shows the form of the Wilkinson curve for the particular Whipple design considered in this report.

The design that was analyzed for this report is as follows. The projectile is assumed to be spherical and composed of 1100-O aluminum. The bumper consists of a 50 mil (0.127 cm) 6061-T6 aluminum sheet. The rear wall consists of a 125 mil (0.3175 cm) 2219-T87 aluminum sheet. The spacing between the bumper and rear wall is taken as 4.0 inches (10.16 cm). Additional parameters necessary to evaluate Equation 1 are $C_s = 5.3$ km/s, $\rho_b = 2.71$ gm/cm³, $\rho_r = 2.71$ gm/cm³, and $\rho = 2.85$ gm/cm³.

Cour-Palais Ballistic Limit Curve

The original Cour-Palais⁵ ballistic limit is referred to as semi-empirical because it relies on a fit to experimental impact data at velocities below ~7 km/s. The extrapolation beyond ~7 km/s is based on scaling of the momentum of the debris cloud. The Cour-Palais ballistic limit curve for velocities greater than 7 km/s is given by:

$$d_c = 4.725 (t_r / V)^{2/3} (S / \rho)^{1/3} (1 / \rho_r)^{1/9} (\sigma / 70)^{1/3}. \quad (2)$$

The terms are defined as

- d_c critical diameter (cm)
- t_r rear wall thickness (cm)

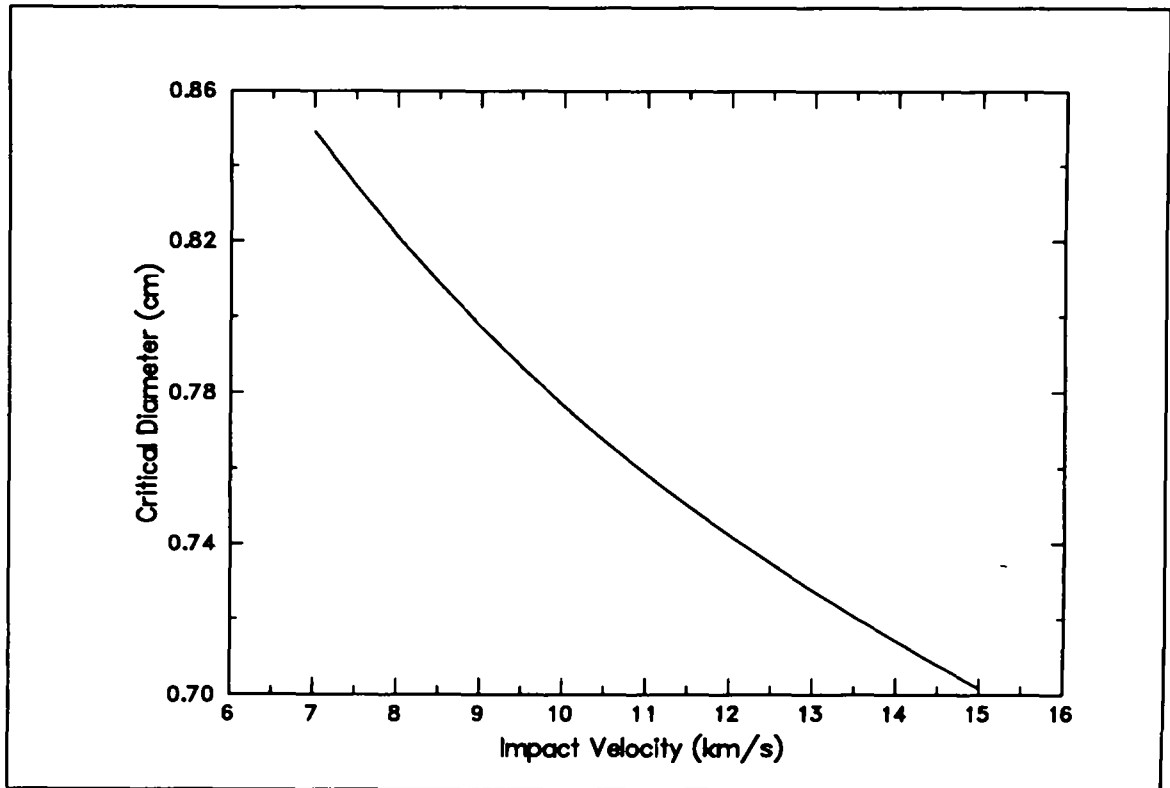


Figure 3. Wilkinson Ballistic Limit for a Whipple Bumper Shield

- ρ_r rear wall density (gm/cm^3)
- V projectile velocity (km/s)
- S bumper-rear wall spacing (cm)
- ρ projectile density (gm/cm^3)
- σ rear wall yield strength (ksi).

Figure 4 shows the form of the Cour-Palais curve for the particular Whipple design considered in this report. For the analysis assumed in this report, the parameters used to evaluate this analytic form are the same as for the Wilkinson curve with the addition of the yield strength for the 2219-T87 aluminum rear wall ($\sigma = 52$ ksi).

Modified Cour-Palais Ballistic Limit Curve

Christiansen⁶ has modified the original Cour-Palais curve to include a fit to the experimental data at velocities below ~ 7 km/s and slightly changed the slope of the curve above ~ 7 km/s. The modified ballistic limit curve is being used for Space Station Freedom design purposes. Again, the extrapolation beyond ~ 7 km/s is based on scaling of the momentum in the debris cloud. The Modified Cour-Palais ballistic limit curve for all

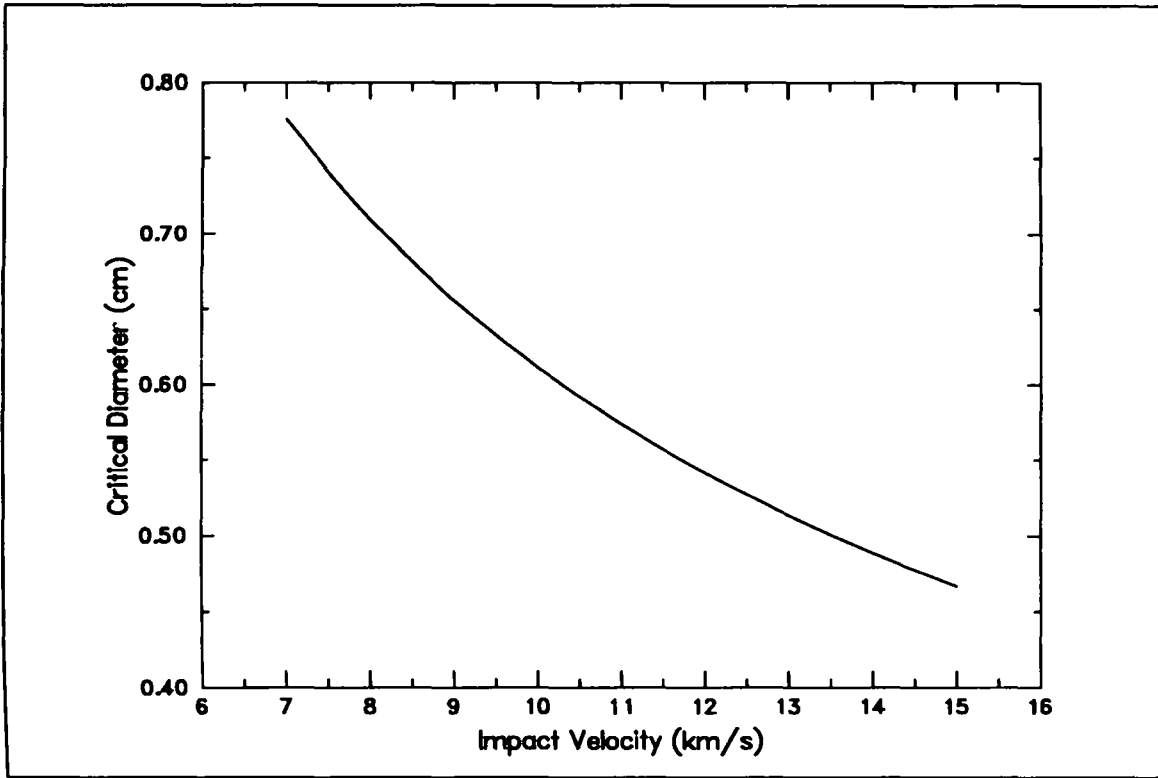


Figure 4. Cour-Palais Ballistic Limit for a Whipple Bumper Shield

velocities is given by:

$$d_c = \left[(t_r \sqrt{\frac{\sigma}{40}} + t_b) / (0.6 \sqrt{\rho_b} V^{2/3}) \right]^{18/19} \quad V \leq 3 \text{ km/s} \quad (3)$$

$$d_c = \left[(t_r \sqrt{\frac{\sigma}{40}} + t_b) / (1.248 \sqrt{\rho_b}) \right]^{18/19} (1.75 - V/4) + \left[1.071 t_r^{2/3} (S/\rho)^{1/3} (1/\rho_r)^{1/9} (\sigma/70)^{1/3} \right] (V/4 - 0.75) \quad 3 \text{ km/s} < V < 7 \text{ km/s} \quad (4)$$

$$d_c = 3.918 (t_r/V)^{2/3} (S/\rho)^{1/3} (1/\rho_r)^{1/9} (\sigma/70)^{1/3} \quad V \geq 7 \text{ km/s} \quad (5)$$

Where the terms are defined as

- d_c critical diameter (cm)
- t_b bumper thickness (cm)
- t_r rear wall thickness (cm)
- ρ projectile density (gm/cm^3)
- ρ_b bumper density (gm/cm^3)
- ρ_r rear wall density (gm/cm^3)
- V projectile velocity (km/s)
- S bumper-rear wall spacing (cm)
- σ rear wall yield strength (ksi).

Figure 5 shows the form of the Modified Cour-Palais curve for the particular Whipple design considered in this report. As before, the same parameters were used to evaluate the analytic form in Figures 5 and 6. Figure 6 shows a comparison of the three ballistic limit curves for the same Whipple. From an inspection of Figure 6, one can note that the differences lie primarily in the absolute location of the curves, not in the slope. All three curves are approaching an asymptote as the velocity increases.

CTH Simulations

CTH Overview

The CTH¹⁰ code was developed to model a wide range of solid dynamics problems involving shock wave propagation and material motion in one, two, or three dimensions: one-dimensional rectilinear, cylindrical, and spherical meshes; two-dimensional rectangular and cylindrical meshes; and three-dimensional rectangular meshes are available. A two-step Eulerian solution scheme is used with these meshes. The first step is a Lagrangian step in which the cells distort to follow the material motion. The second step

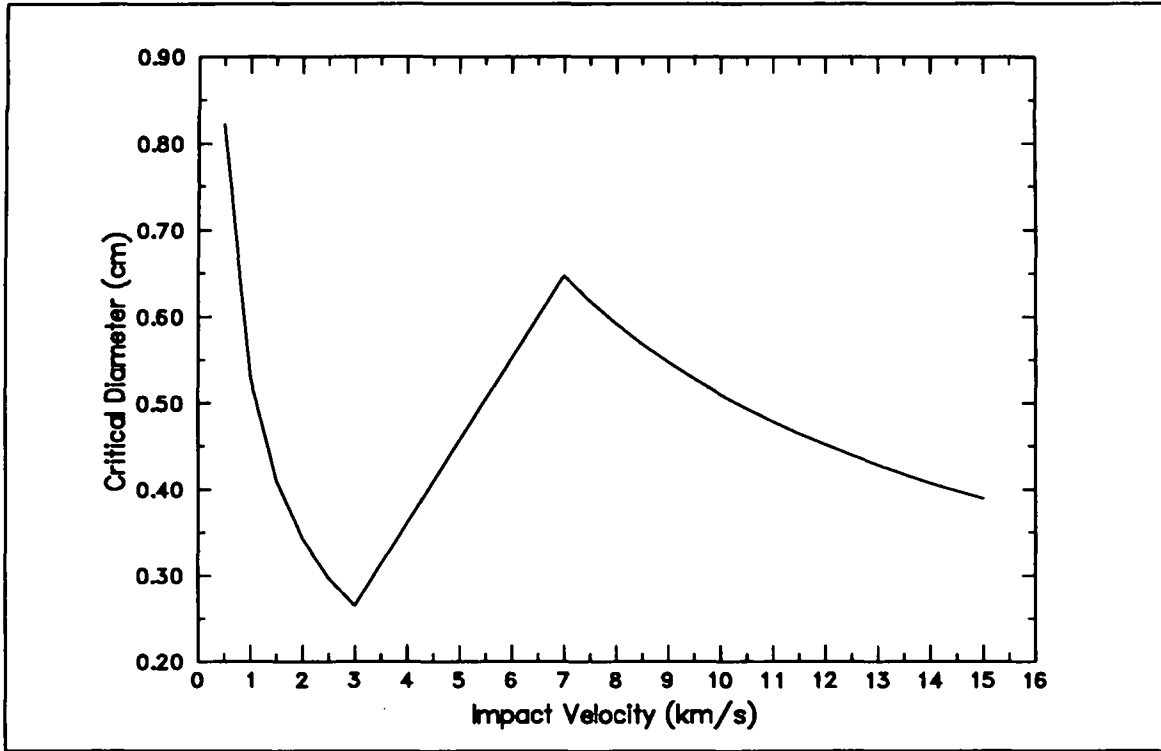


Figure 5. Modified Cour-Palais Ballistic Limit for a Whipple Bumper Shield

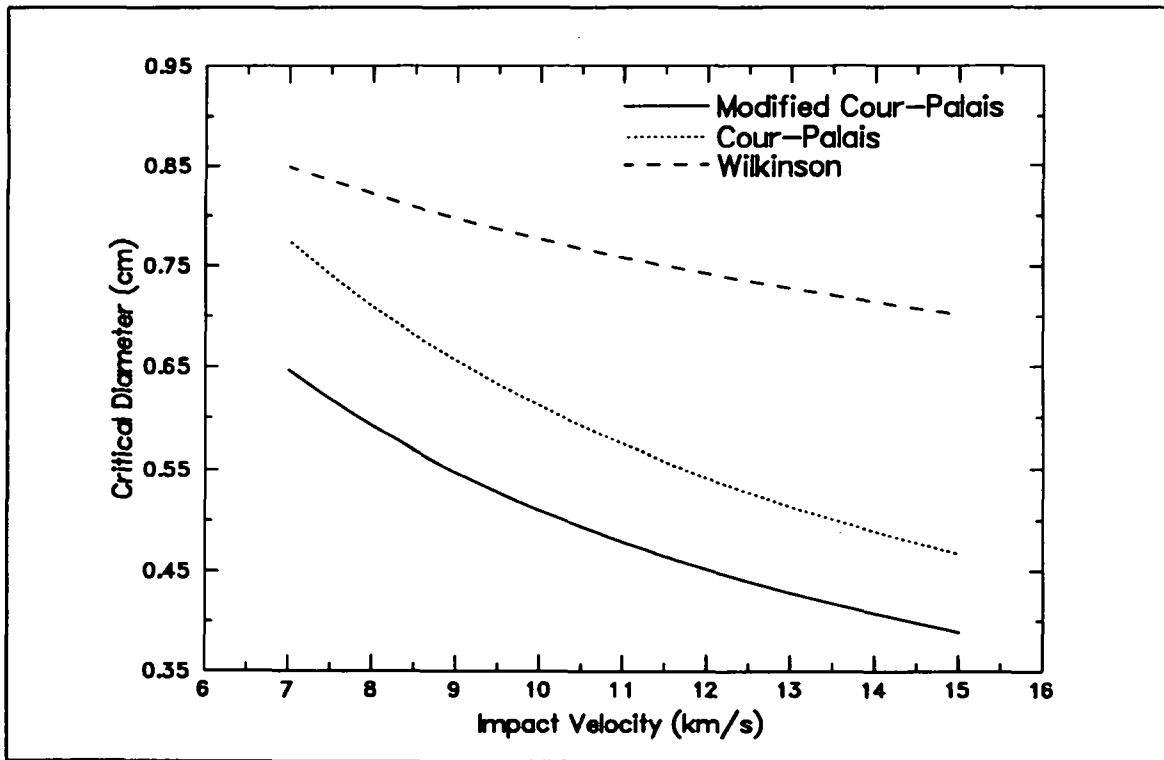


Figure 6. A Comparison of Three Ballistic Limit Curves above 7 km/s

is a remesh step where the distorted cells are mapped back to the original Eulerian mesh.

CTH has several thermodynamic models that are used for simulating strong shock, large deformation events. Both tabular and analytic equations-of-state are available. CTH can model elastic-plastic behavior, high explosive detonation, fracture, and motion of fragments smaller than a computational cell. The elastic-plastic model is linearly elastic-perfectly plastic with thermal softening. A programmed burn model is available for simulating high explosive detonation with ideal gas and Jones-Wilkins-Lee equations-of-state available for computing the thermodynamic properties of high explosive reaction products. A special model is available for moving fragments smaller than a computational cell with the correct statistical velocity. CTH has been carefully designed to minimize the dispersion generally found in Eulerian codes. It has a high-resolution interface tracker that prevents breakup and distortion of material interfaces. It uses second-order convection schemes to flux all quantities between cells.

Computational Technique

Six of the seven CTH simulations assumed normal impacts. The computational geometry used to simulate the normal impacts was two-dimensional axisymmetric. All six simulations used identical zoning, material strength models, and equations-of-state. One CTH simulation was completed to assess the effects of oblique impacts. An impact angle of 45° was chosen for this single three dimensional simulation. The computational geometry used to simulate the oblique impact was three-dimensional rectangular. Table 1 lists the velocity, mass, and projectile diameter for the seven CTH simulations. The

Table 1. Projectile Parameters for the CTH Simulations

CTH Model	Ballistic Limit Curve	Velocity (km/s)	Mass (gm)	Diameter (cm)
na8-w	Wilkinson	8.0	0.727	0.80
na8-mcp	Cour-Palais	8.0	0.487	0.70
na10-w	Wilkinson	10.0	0.674	0.78
na10-mcp	Cour-Palais	10.0	0.338	0.62
na12-w	Wilkinson	12.0	0.552	0.73
na12-mcp	Cour-Palais	12.0	0.224	0.54
na12-ob	Cour-Palais	12.0	0.224	0.54

diameters were chosen by evaluating the Wilkinson or modified Cour-Palais analytic expressions for velocities of 8, 10, and 12 km/s.

The six axisymmetric simulations used the following numerical resolution. The radial (x-coordinate) zoning starts at 0.0 and consisted of constant zones of width 0.015 cm over a region 1.0 cm wide. A second region of radial zoning starts at 2.0 cm, ends at 9.0 cm, and consists of increasing zone size from 0.015 cm to 0.400 cm. The third region starts at 9.0 cm and consists of increasing zone size from 0.400 cm to 0.800 cm to a radius of

Comparison of Analytic Whipple Bumper Shield Ballistic Limits with CTH Simulations

15.0 cm. The axial (y-coordinate) zoning starts at -1.0 cm consists of decreasing zone size from 0.030 cm to 0.015 cm at a position of 0.0 cm. A second region of axial zoning starts at 0.0 cm and consists of constant zones of length 0.015 cm over a region 1.0 cm long. A third region of axial zoning starts at 1.0 cm and consists of increasing zone size from 0.015 cm to 0.075 cm at a position of 6.0 cm. A fourth region of axial zoning starts at 6.0 cm and consists of decreasing zone size from 0.075 cm to 0.015 cm at a position of 11.0 cm. The last region of axial zoning starts at 11.0 cm and consists of constant zones of length 0.015 cm over a region 3.0 cm long. This method of zoning the simulations allows for good resolution (~10 zones across the axial dimension) of the relatively thin bumper and excellent resolution (~25 zones across the axial dimension) in the rear wall. In addition, for full second-order accuracy, the zoning is square in those regions of primary importance in the bumper and the rear wall. A sample CTH input deck is reproduced in Appendix A.

The single three-dimensional simulation started with the zoning as described in Tables 2 thru 4. To improve the computational efficiency, the simulation was rezoned at 9 μ s. The zoning used after the rezone is described in Tables 5 through 7. This method of zoning the simulations allows for good resolution (~10 zones) of the relatively thin bumper and in the rear wall. In addition, for full second order accuracy, the zoning is square in those regions of primary importance in the bumper and the rear wall. The initial CTH input deck is reproduced in Appendix B.

Table 2. Initial X Zoning

X_{low}	X_{high}	ΔX_{low}	ΔX_{high}
-8.0	-2.0	0.350	0.100
-2.0	-0.4	0.100	0.030
-0.4	+0.4	0.030	0.030
+0.4	+2.0	0.030	0.100
+2.0	+8.0	0.100	0.350

Table 3. Initial Y Zoning

Y_{low}	Y_{high}	ΔY_{low}	ΔY_{high}
-1.000	-0.600	0.070	0.055
-0.600	0.000	0.055	0.031
0.000	+0.124	0.031	0.031
+0.124	+5.200	0.031	0.250
+5.200	+10.287	0.250	0.040

Table 3. Initial Y Zoning

Y_{low}	Y_{high}	ΔY_{low}	ΔY_{high}
+10.287	+10.927	0.040	0.040
+10.927	+12.927	0.040	0.100

Table 4. Initial Z Zoning

Z_{low}	Z_{high}	ΔZ_{low}	ΔZ_{high}
+0.0	+0.42	0.03	0.03
+0.42	+2.02	0.03	0.10
+2.02	+8.02	0.10	0.35

Table 5. Final X Zoning

X_{low}	X_{high}	ΔX_{low}	ΔX_{high}
-5.0	0.0	0.40	0.20
0.0	+4.0	0.20	0.04
+4.0	+6.0	0.04	0.04
+6.0	+8.0	0.04	0.06
+8.0	+12.0	0.06	0.25

Table 6. Final Y Zoning

Y_{low}	Y_{high}	ΔY_{low}	ΔY_{high}
+1.000	+10.287	0.40	0.04
+10.287	+10.927	0.04	0.04
+10.927	+14.000	0.04	0.18

Table 7. Final Z Zoning

Z_{low}	Z_{high}	ΔZ_{low}	ΔZ_{high}
+0.0	+1.0	0.04	0.04
+1.0	+3.0	0.04	0.08
+3.0	+9.0	0.08	0.35

All materials were treated using a linearly-elastic perfectly-plastic model of material

Comparison of Analytic Whipple Bumper Shield Ballistic Limits with CTH Simulations

strength with a von Mises yield surface. Principal stress was used to trigger the void insertion fracture model for all materials. The projectile was treated as 1100-O aluminum alloy. The bumper was treated as an 6061-T6 aluminum alloy. The rear wall was treated as an 2219-T87 aluminum alloy. Table 8 lists the yield and tensile strengths and densities for the three aluminum alloys considered here. The values chosen for these simulations were not taken from a specific reference, but was chosen based on the collective experience of several analysts and are felt to be appropriate for the simulations. The values that were used reflect the well known increase in yield^{11,12} and fracture strength in a dynamic loading environment.

Table 8. Strength Parameters used for CTH Simulations

Aluminum Type	Static Yield (dynes/cm ²)	Dynamic Yield (dynes/cm ²)	Fracture Strength (dynes/cm ²)	Density (gm/cm ³)
1100-O	3.4x10 ⁸	1.0x10 ⁹	1.0x10 ⁹	2.712
6061-T6	2.8x10 ⁹	5.0x10 ⁹	11.0x10 ⁹	2.712
2219-T87	3.9x10 ⁹	7.0x10 ⁹	15.0x10 ⁹	2.851

The projectile and bumper were represented by the equation-of-state developed by Kerley¹³ and validated against experimental data for pressures below 80 GPa. The 2219 form of aluminum was also represented by the same equation-of-state with an adjustment made to reflect the higher initial density of the 2219-T87 aluminum alloy. This form of the equation-of-state for aluminum is considered to be one of the best available to represent the solid-liquid and liquid-vapor phase changes.

CTH Results

Normal Impact

The six axisymmetric simulations were run to problem times of 25 to 30 μ s, depending on the impact velocity. In all cases, at the end of the computational record, the debris cloud was examined to determine the potential for further damage to the rear wall. It was determined that the debris cloud created from the initial impact had completely interacted with the rear wall and had rebounded. Due to these facts, it is felt that no further damage to the rear wall by the debris cloud can be expected from the impact. That does not preclude a late time structural failure due to the impulse of the debris impact. Hydrodynamic codes like CTH are not generally capable of accurately determining late time structural effects which are dominated by the details of the material strength models.

Using the results of the CTH simulations, a determination of penetration/no-penetration was made. Table 9 lists the results of this determination. Since the projectile diameter

Table 9. CTH Penetration Predictions for the Axisymmetric Simulations

CTH Model	Ballistic Limit Curve	Velocity (km/s)	Diameter (cm)	Penetration Y/N
na8-w	Wilkinson	8.0	0.80	Y
na8-mcp	Cour-Palais	8.0	0.70	N
na10-w	Wilkinson	10.0	0.78	Y
na10-mcp	Cour-Palais	10.0	0.62	N
na12-w	Wilkinson	12.0	0.73	N
na12-mcp	Cour-Palais	12.0	0.54	N

chosen was taken from the respective ballistic limit curve, one would expect the CTH penetration predictions would scatter about both curves.

The debris clouds were examined to estimate the thermodynamic state of the debris cloud. Table 10 lists the mass percentages in the liquid state ($960\text{ K} > T < 2700\text{ K}$) and the vapor state ($T > 2700\text{ K}$) for the projectile and bumper material in the debris cloud. These estimates were taken just prior to impact by the debris cloud on the rear wall. An inspection

Table 10. CTH Estimates of the Thermodynamic State of the Debris Cloud

CTH Model	% Solid Bumper	% Liquid Bumper	% Vapor Bumper	% Solid Projectile	% Liquid Projectile	% Vapor Projectile
na8-w	21	77	2	67	33	0
na8-mcp	26	73	1	36	64	0
na10-w	12	88	0	35	65	0
na10-mcp	0	100	0	35	65	0
na12-w	0	83	17	26	35	39
na12-mcp	0	83	17	37	41	12

of Table 10 indicates that the vapor percentages increase as the impact velocity increases, as anticipated.

Finally, the next series of figures shows a representation of the debris cloud and the terminal rear wall damage for each of the CTH simulations. Each simulation is represented by three figures, the first image is taken at ~4 cm behind the bumper, the second image is taken just before impact with the rear wall, and the third image is taken at the end of the

Comparison of Analytic Whipple Bumper Shield Ballistic Limits with CTH Simulations

computational record if the rear wall is not perforated or just after perforation of the rear wall. Figures 7 through 24 display the same information, the right side of the frame contains

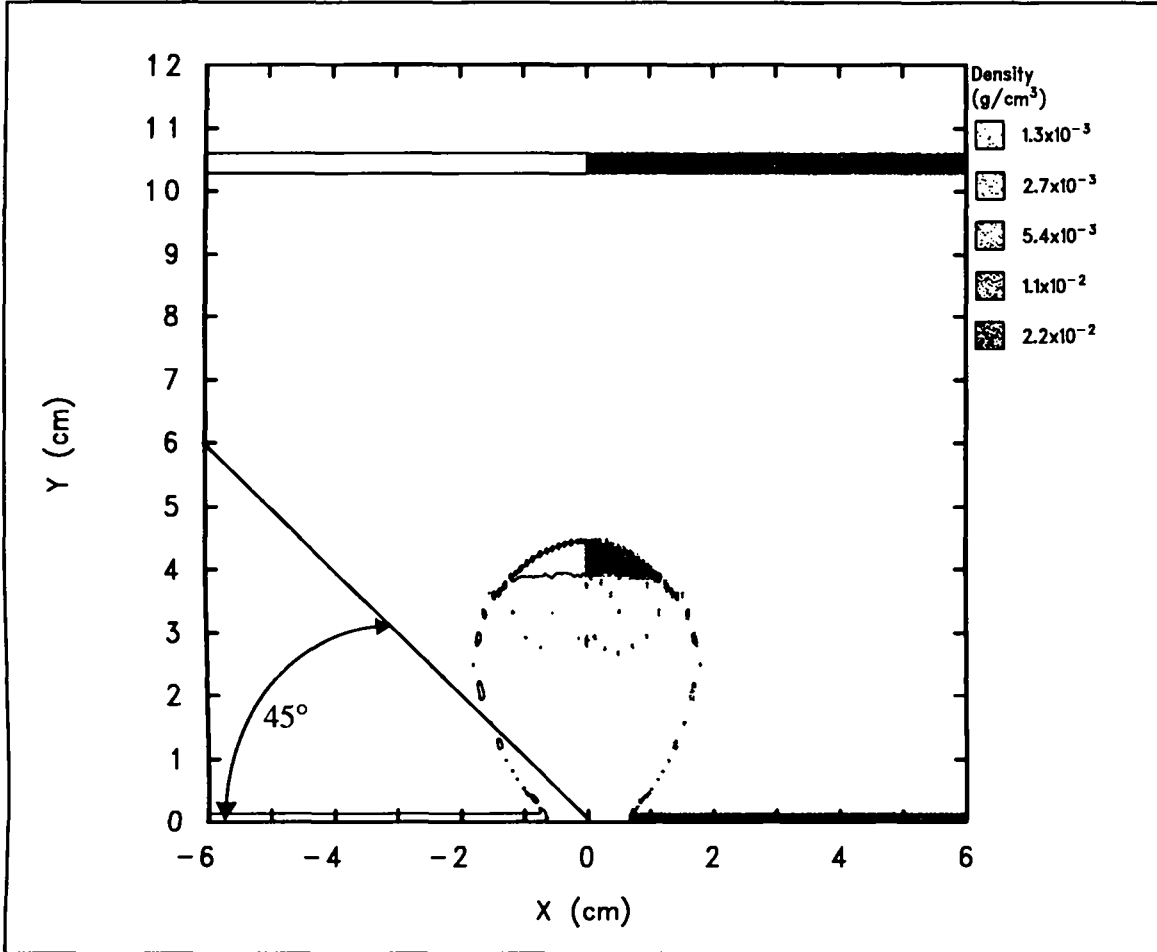


Figure 7. The na8-w CTH Simulation Halfway Between the Bumper and Rear Wall

a representation of the density. The cell density is scaled by the “density” of dots as represented in the legend in each frame. In addition, the “interface” lines are also drawn, the “interface” is defined to be a contour line (value = 0.5) of the volume fraction for each material. On the left side of the frame, only the “interface” lines are drawn. The apparent cross-section displayed in the above and following figures is an artifact of the graphics package, that is, the combination of right and left side information in the same frame, and not a true cross-section of a debris cloud.

The debris clouds are very similar for the six simulations considered here. All show roughly spherical propagation fronts with the spray angles ranging from $\sim 40^\circ$ to $\sim 45^\circ$. The most significant difference correlates with the vapor/liquid percentages from Table 10. As the impact velocity increases, the vapor content of the projectile material increases. This can be seen in the difference in the interface lines for Figures 8 and 20. In all cases, the debris cloud has the original bumper material on the leading edge. This feature is most evident in Figures 8, 11, 14, 17, 20, and 23. The original bumper material tends to form “fingers” (see A in Figure 8) in the direction of motion, this is due to the aspect ratio of the zoning in

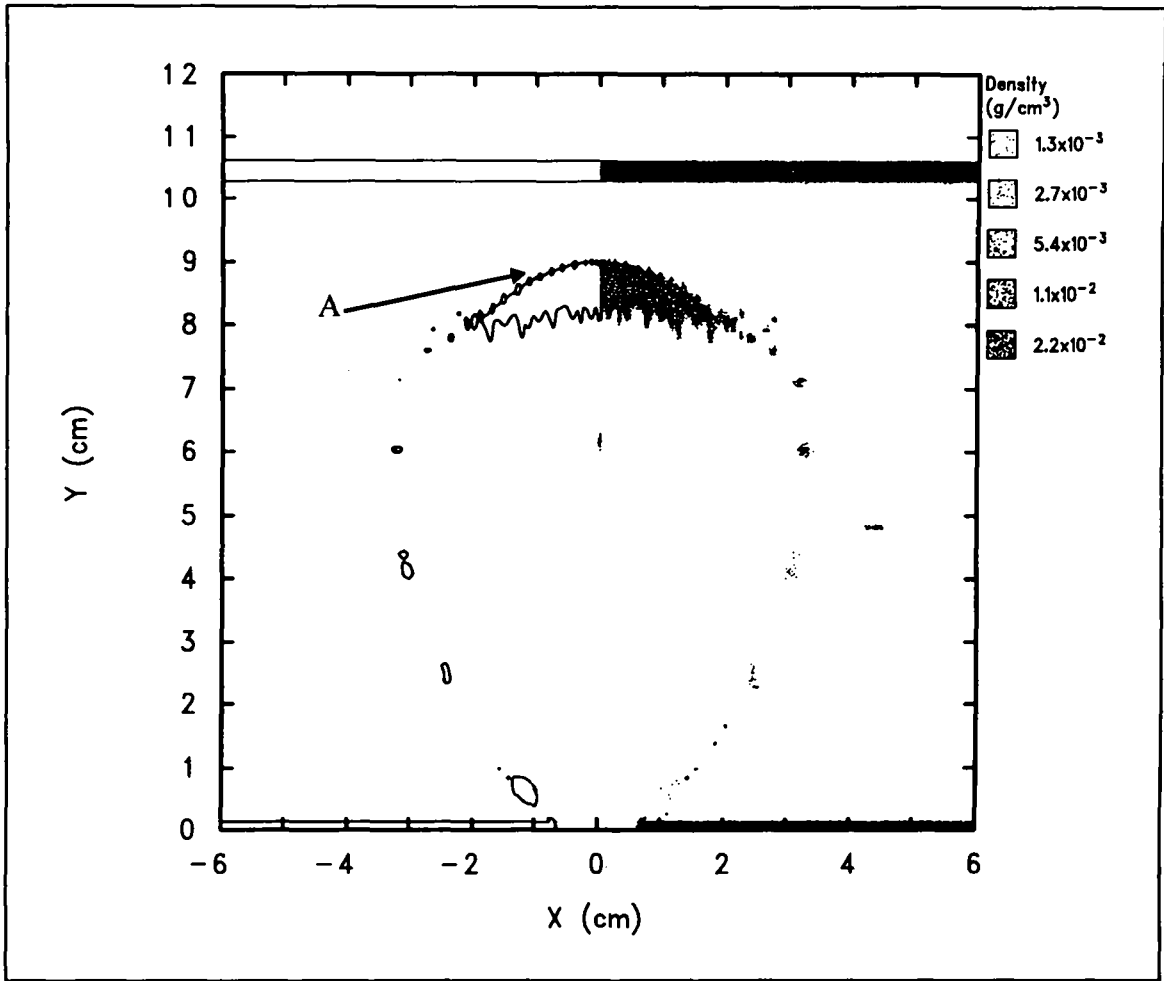


Figure 8. The na8-w CTH Simulation Just Before Rear Wall Impact

the region between the bumper and rear wall. Analyses of other simulations indicate that the aspect ratio of zones in the intermediate region do not significantly affect the terminal rear wall damage.

Comparison of Analytic Whipple Bumper Shield Ballistic Limits with CTH Simulations

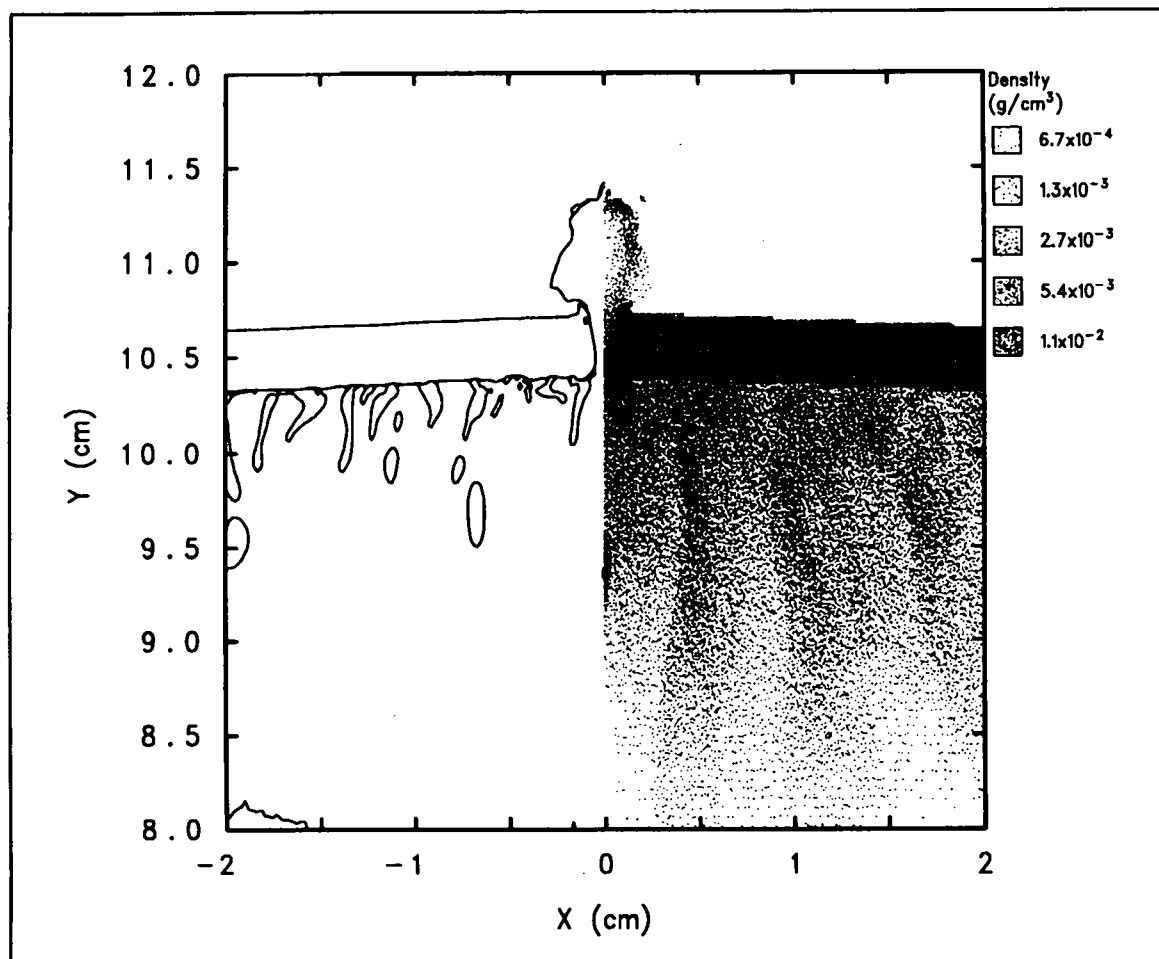


Figure 9. The na8-w CTH Simulation Rear Wall Terminal Damage

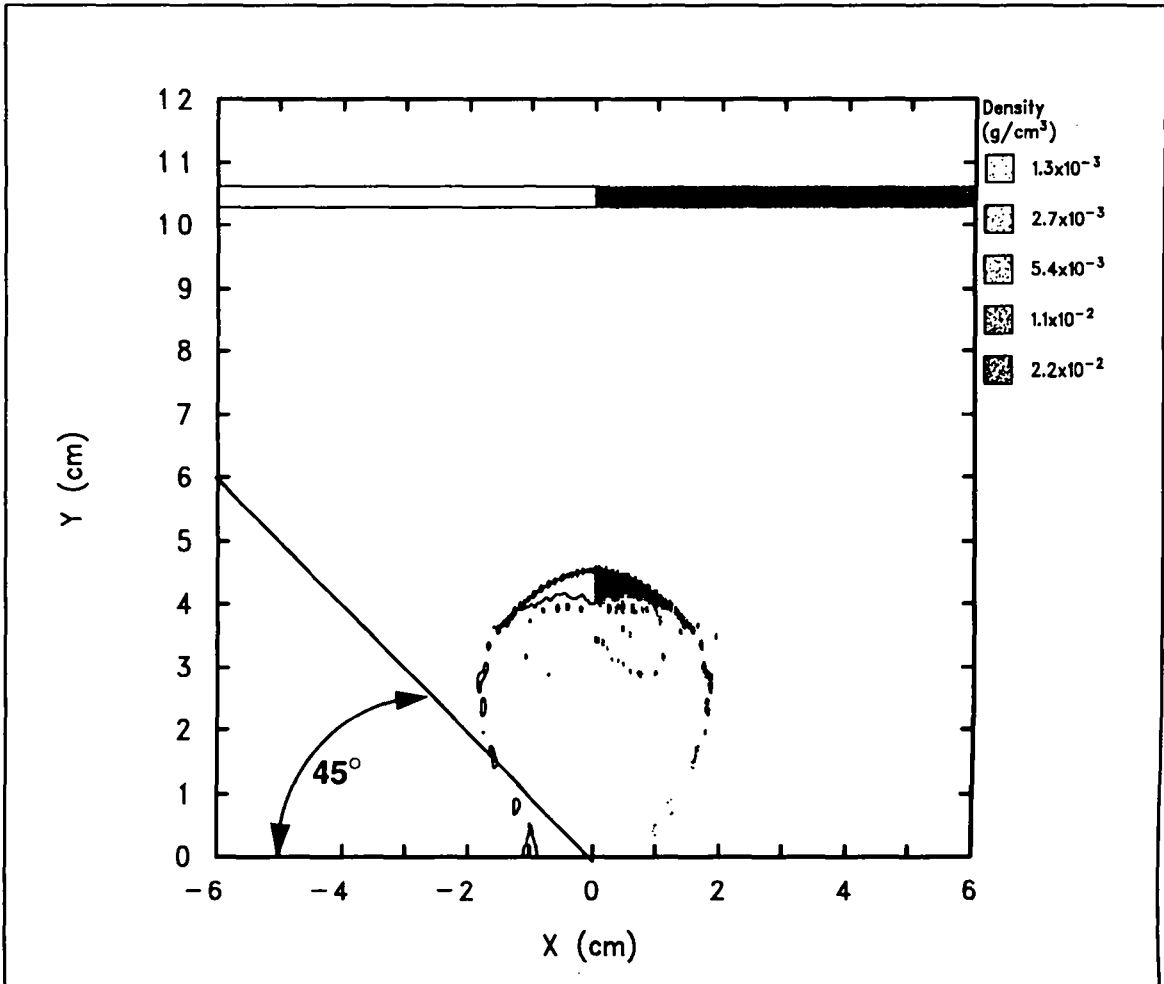


Figure 10. The na8-mcp CTH Simulation Halfway Between the Bumper and Rear Wall

Comparison of Analytic Whipple Bumper Shield Ballistic Limits with CTH Simulations

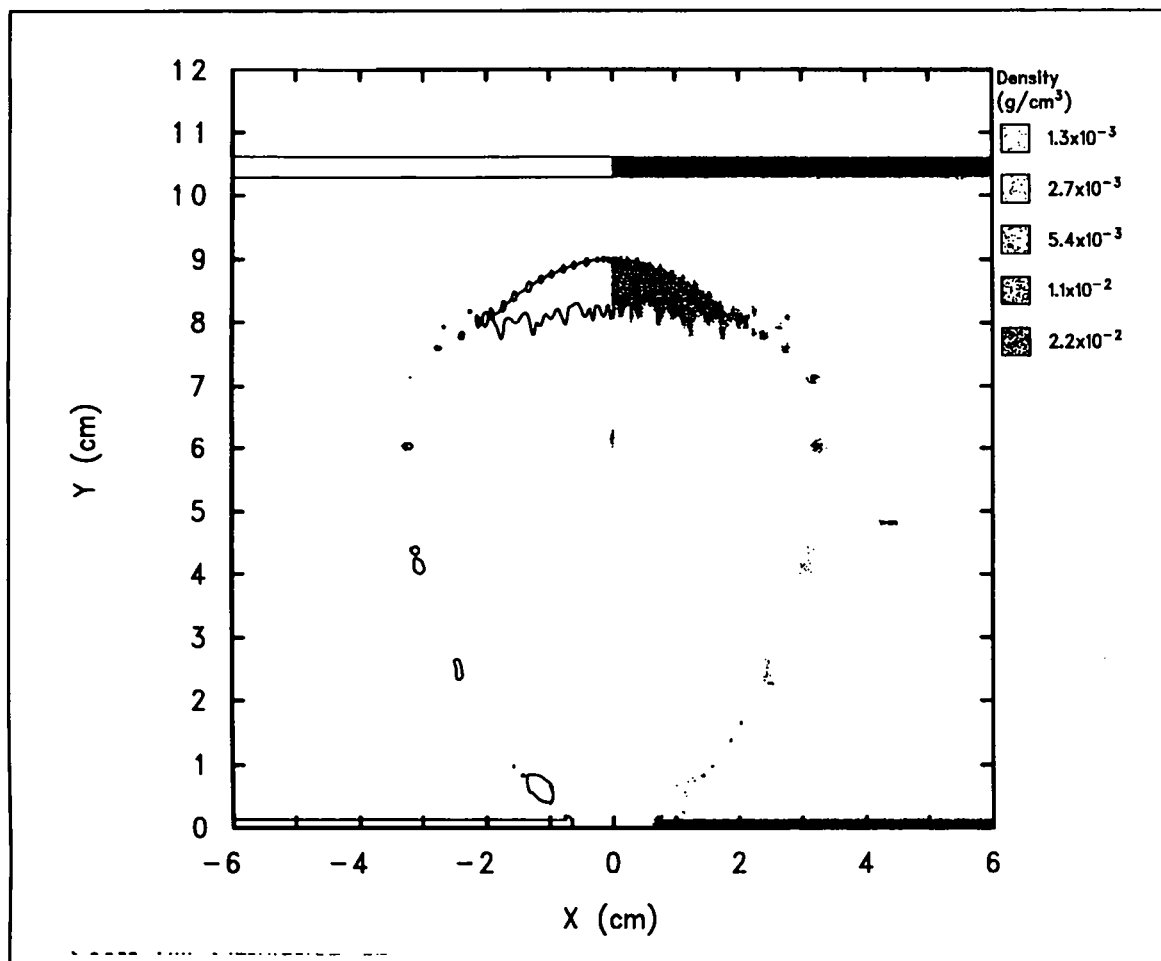


Figure 11. The na8-mcp CTH Simulation Just Before Rear Wall Impact

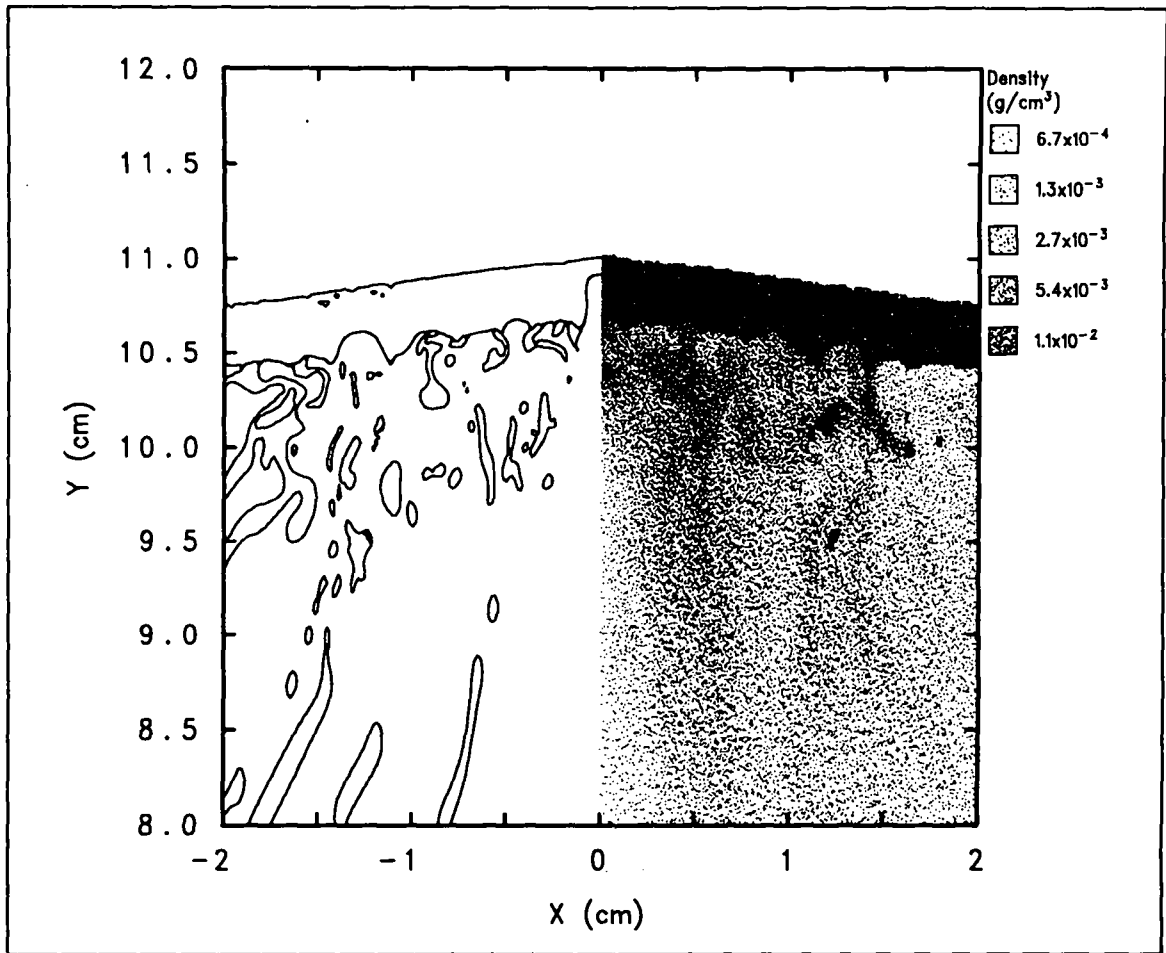


Figure 12. The na8-mcp CTH Simulation Rear Wall Terminal Damage

Comparison of Analytic Whipple Bumper Shield Ballistic Limits with CTH Simulations

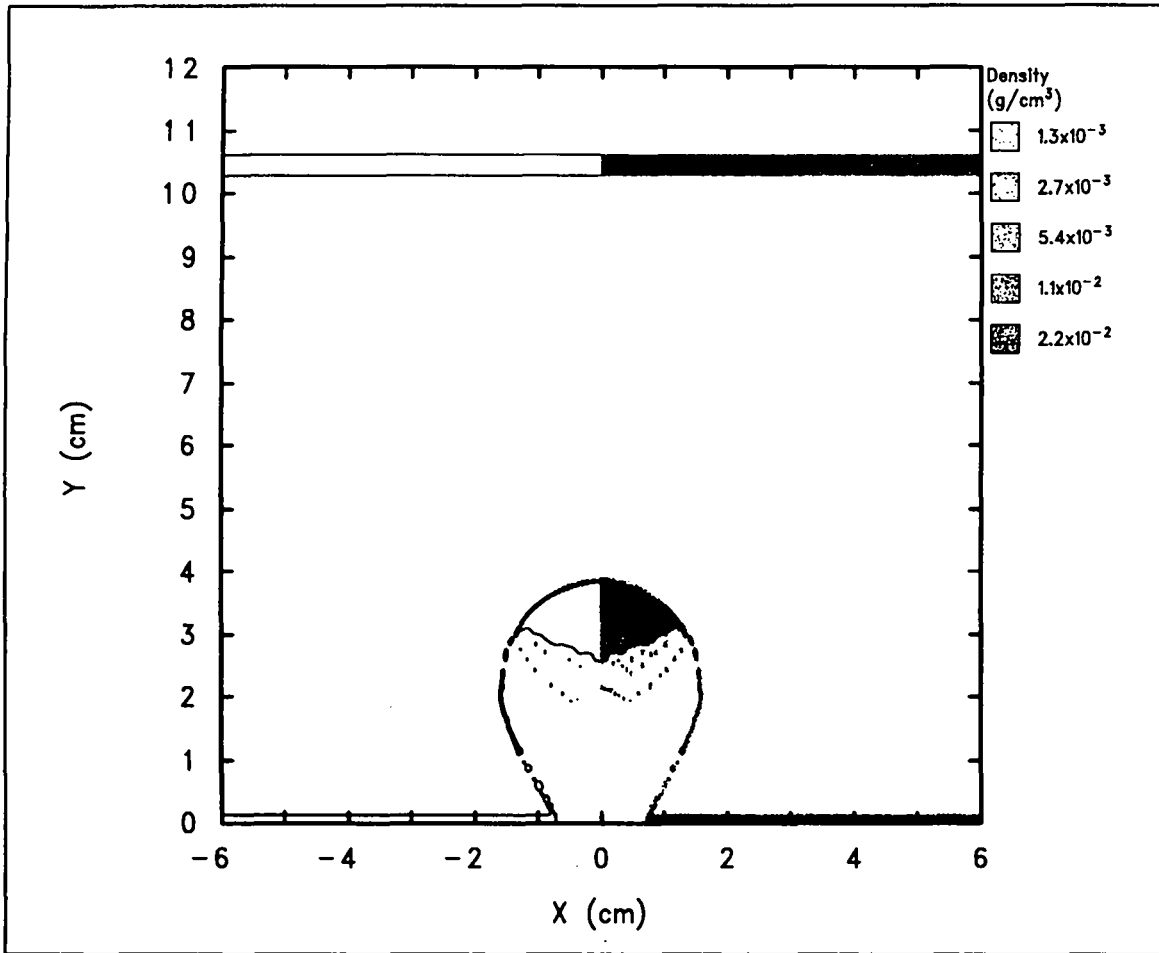


Figure 13. The na10-w CTH Simulation Halfway Between the Bumper and Rear Wall

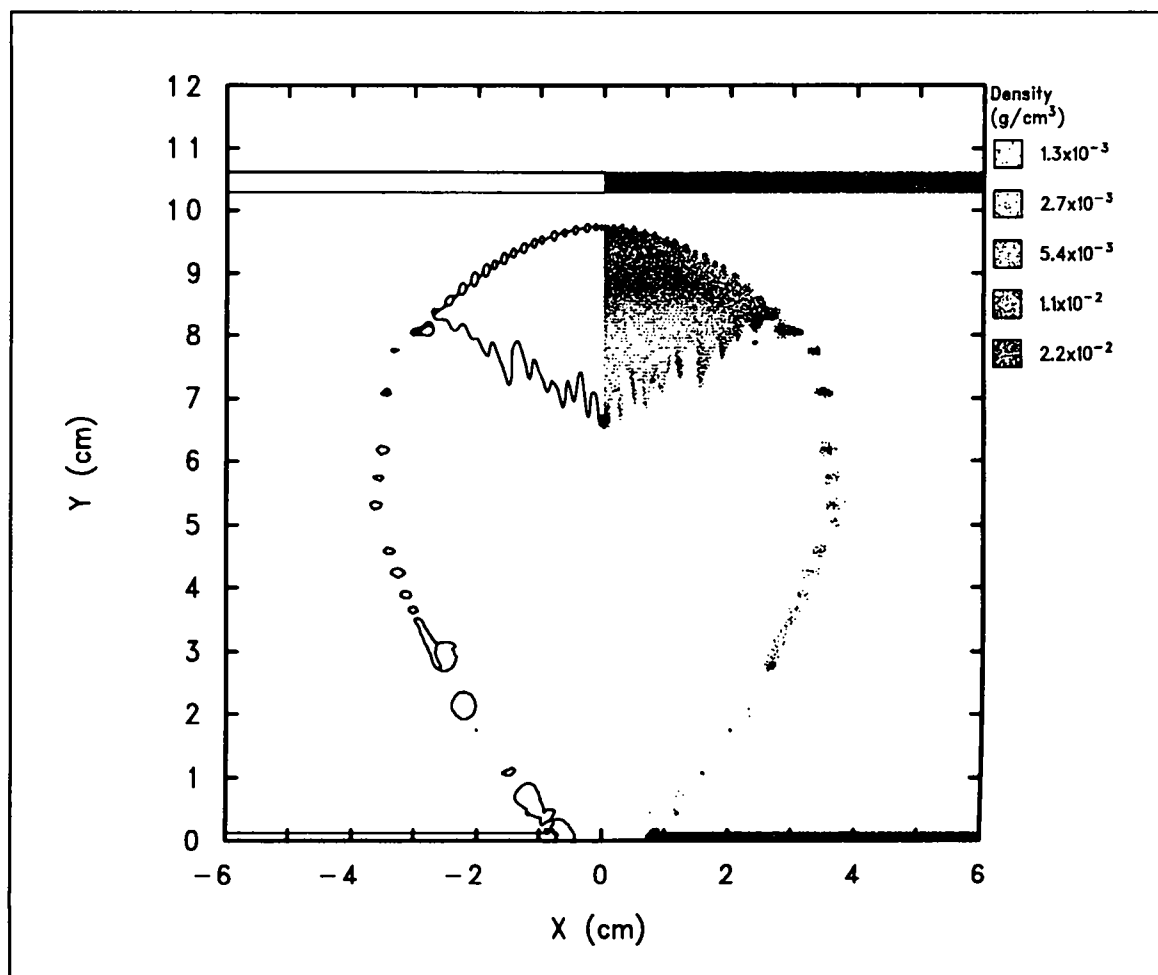


Figure 14. The na10-w CTH Simulation Just Before Rear Wall Impact

Comparison of Analytic Whipple Bumper Shield Ballistic Limits with CTH Simulations

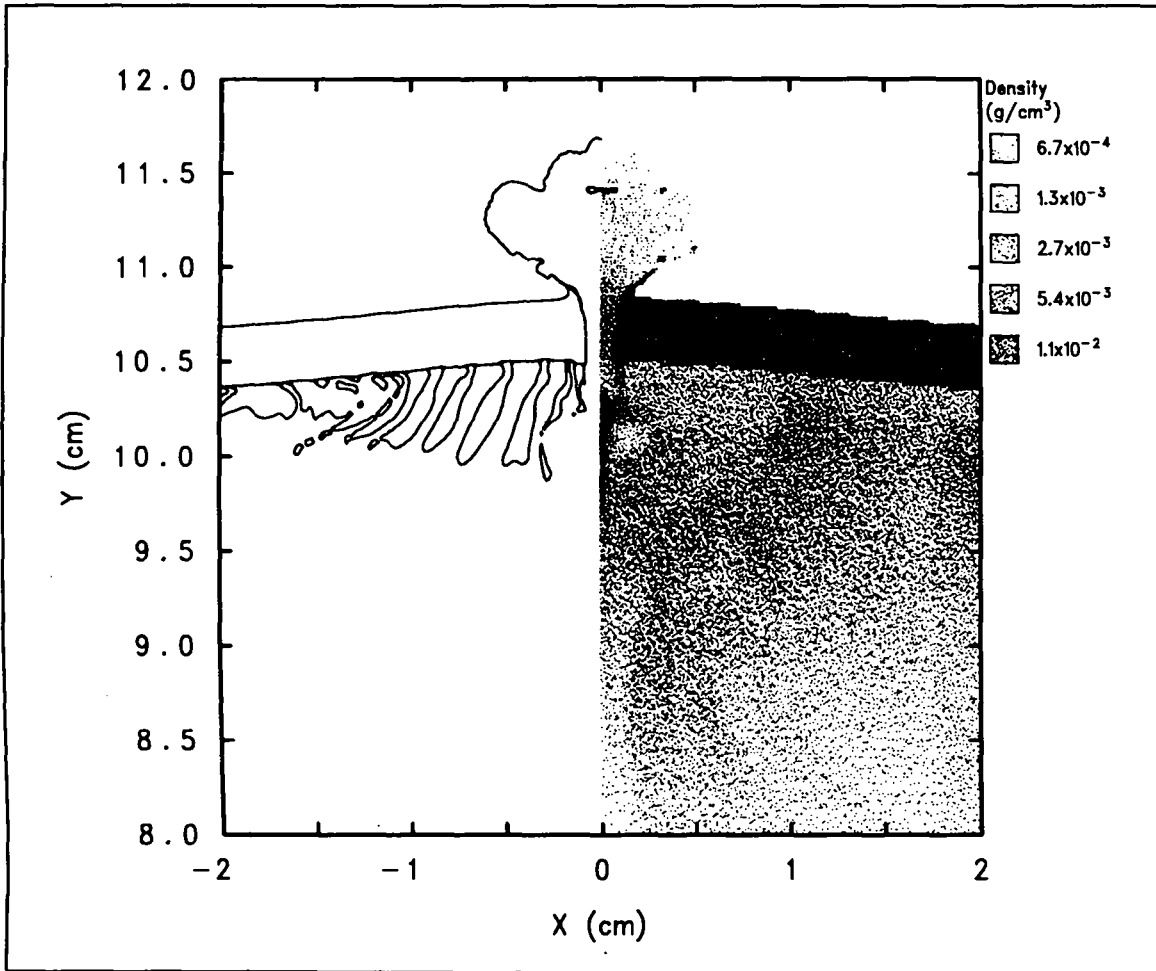


Figure 15. The na10-w CTH Simulation Rear Wall Terminal Damage

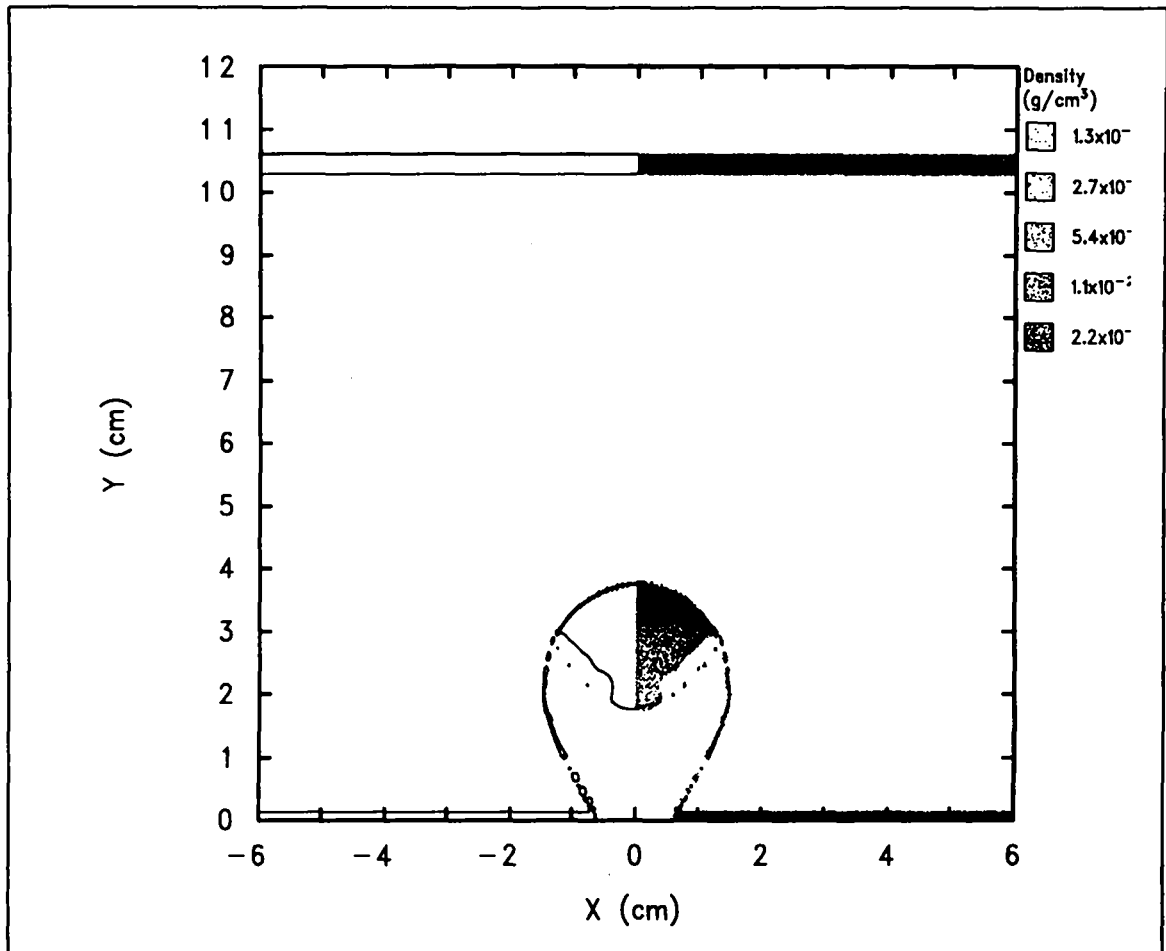


Figure 16. The na10-mcp CTH Simulation Halfway Between the Bumper and Rear Wall

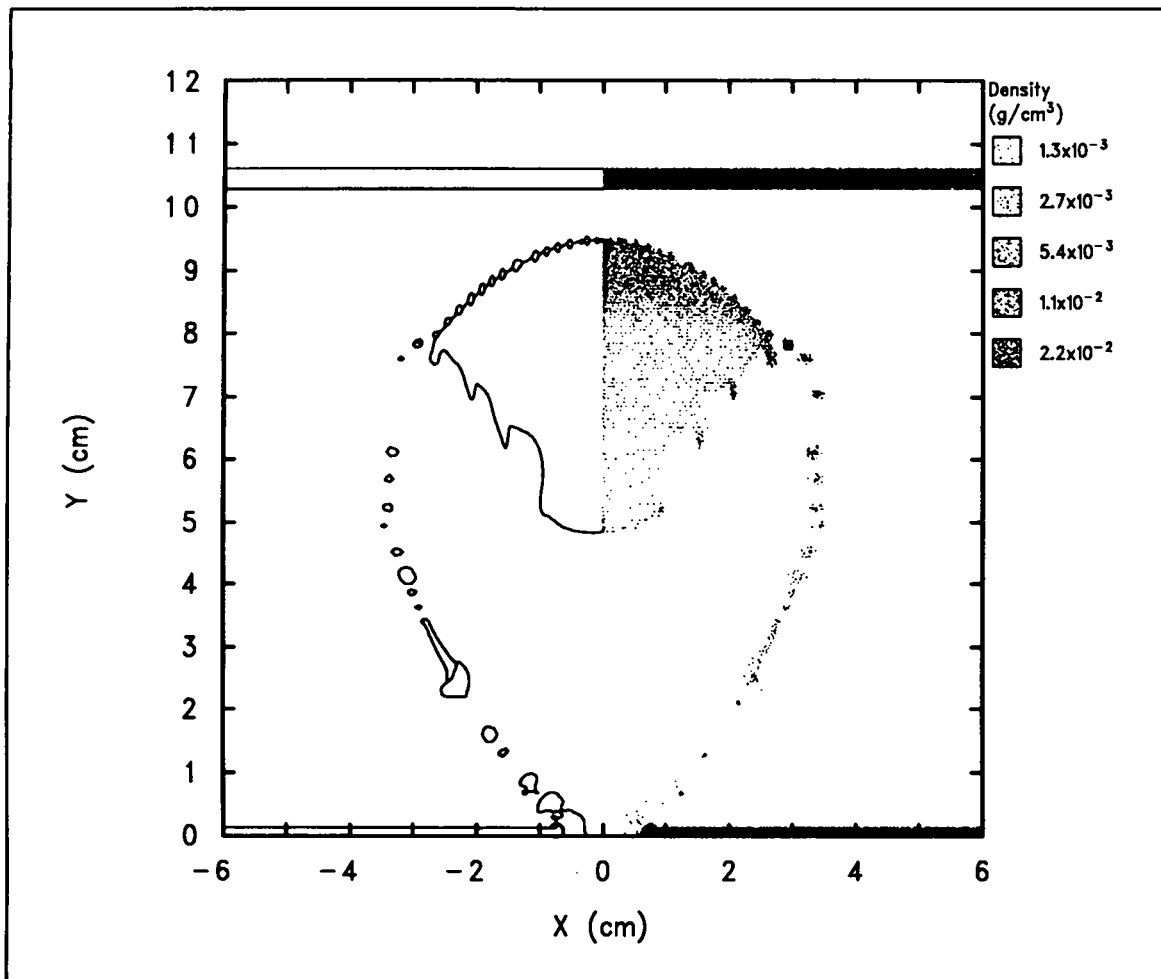


Figure 17. The na10-mcp CTH Simulation Just Before Rear Wall Impact

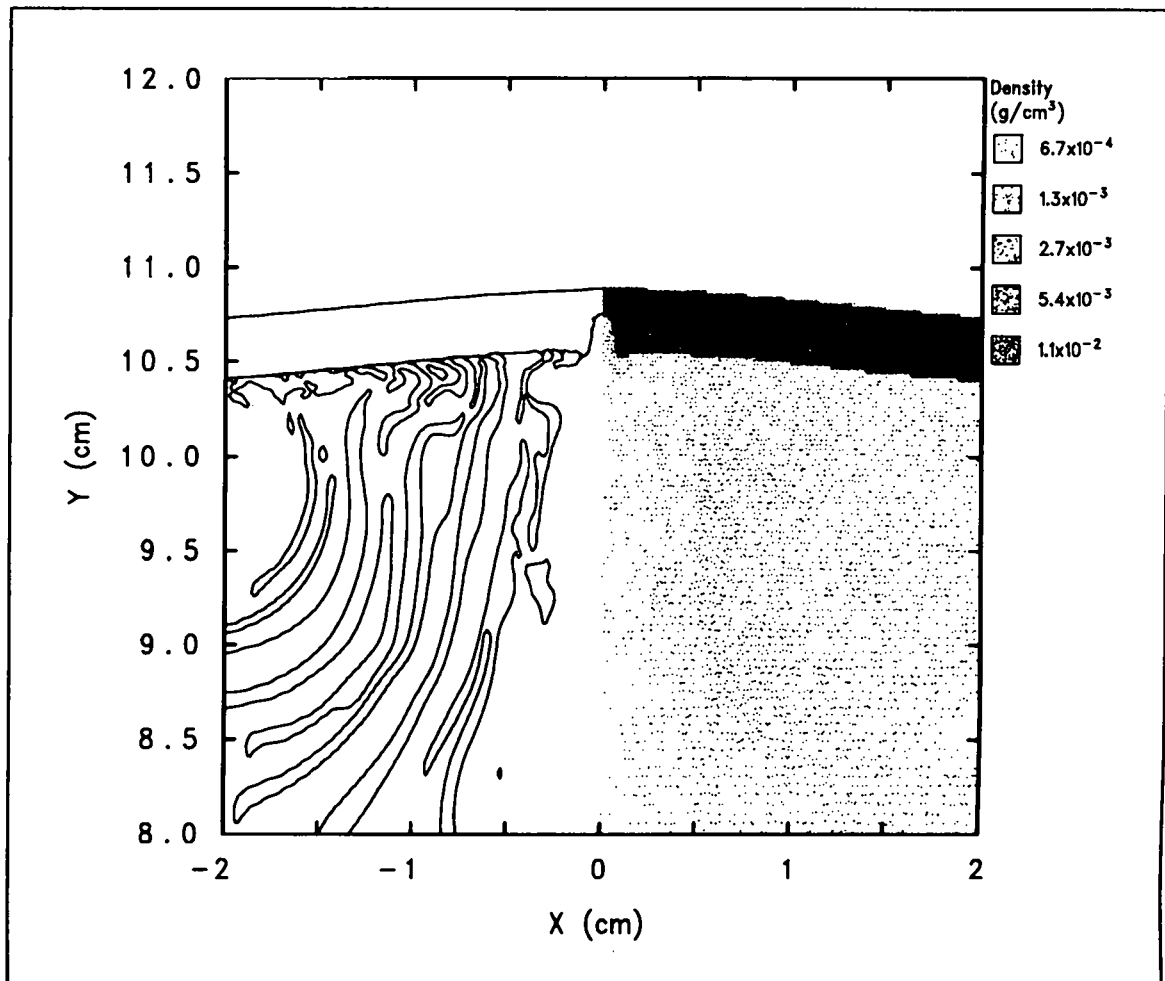


Figure 18. The na10-mcp CTH Simulation Rear Wall Terminal Damage

Comparison of Analytic Whipple Bumper Shield Ballistic Limits with CTH Simulations

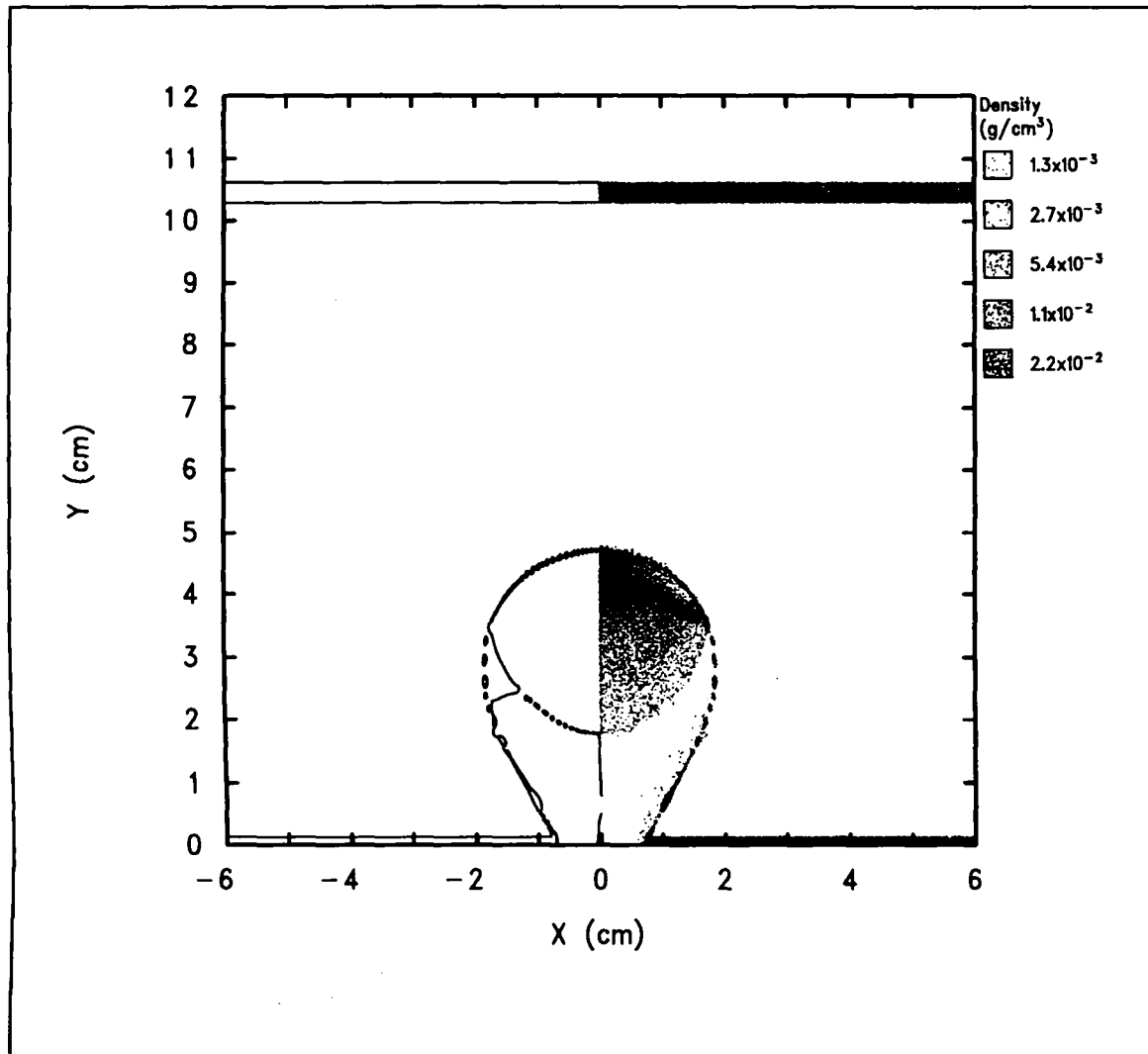


Figure 19. The na12-w CTH Simulation Halfway Between the Bumper and Rear Wall

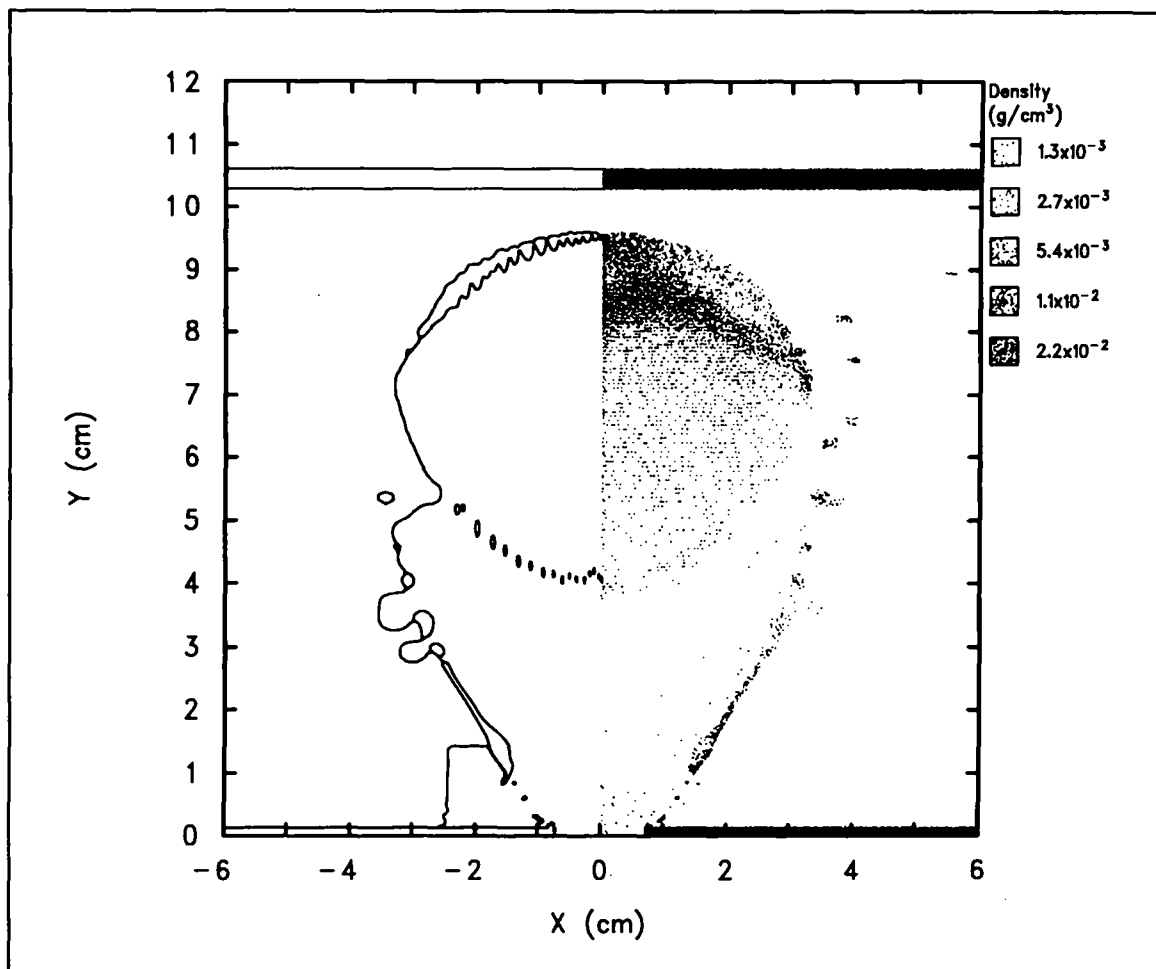


Figure 20. The na12-w CTH Simulation Just Before the Rear Wall

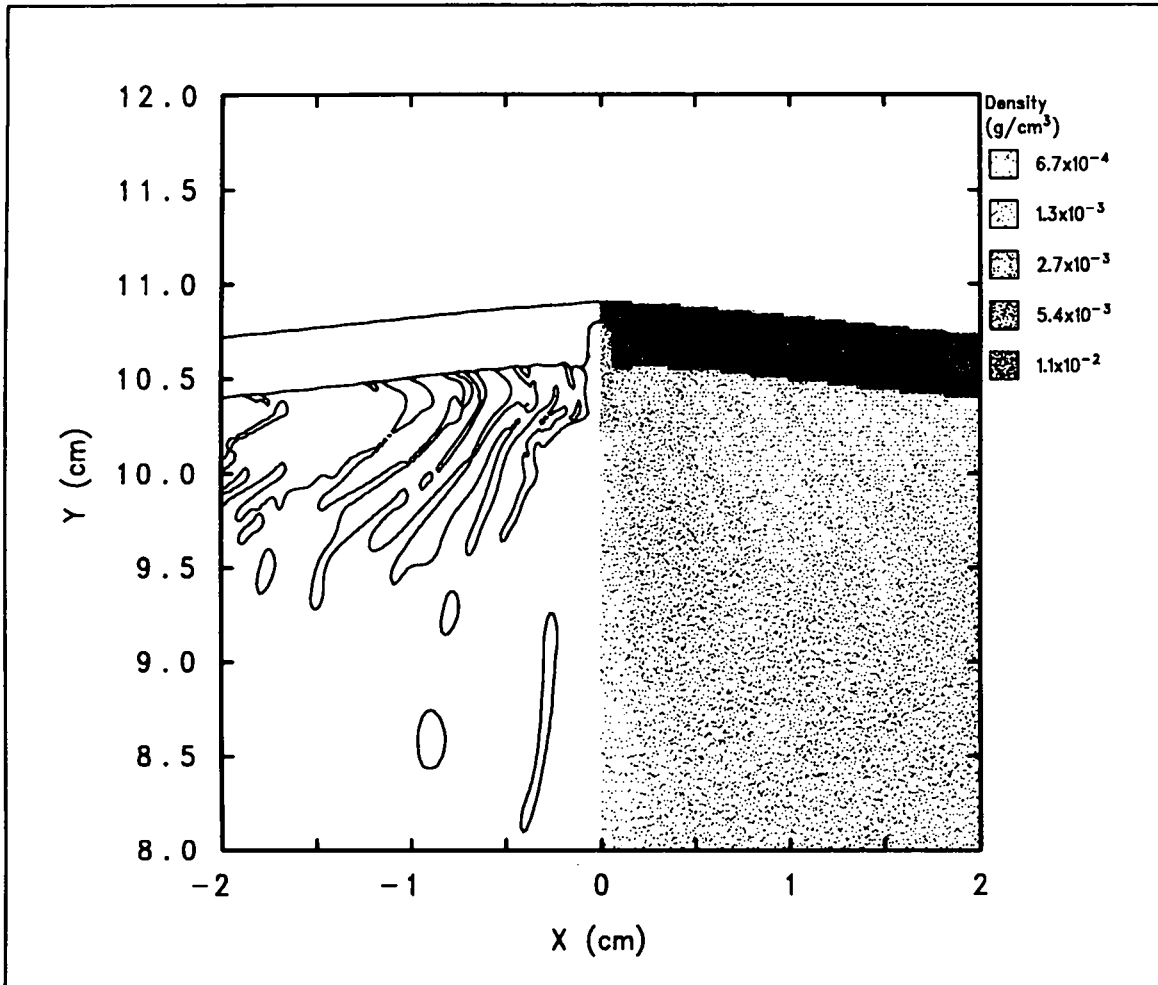


Figure 21. The na12-w CTH Simulation Rear Wall Terminal Damage

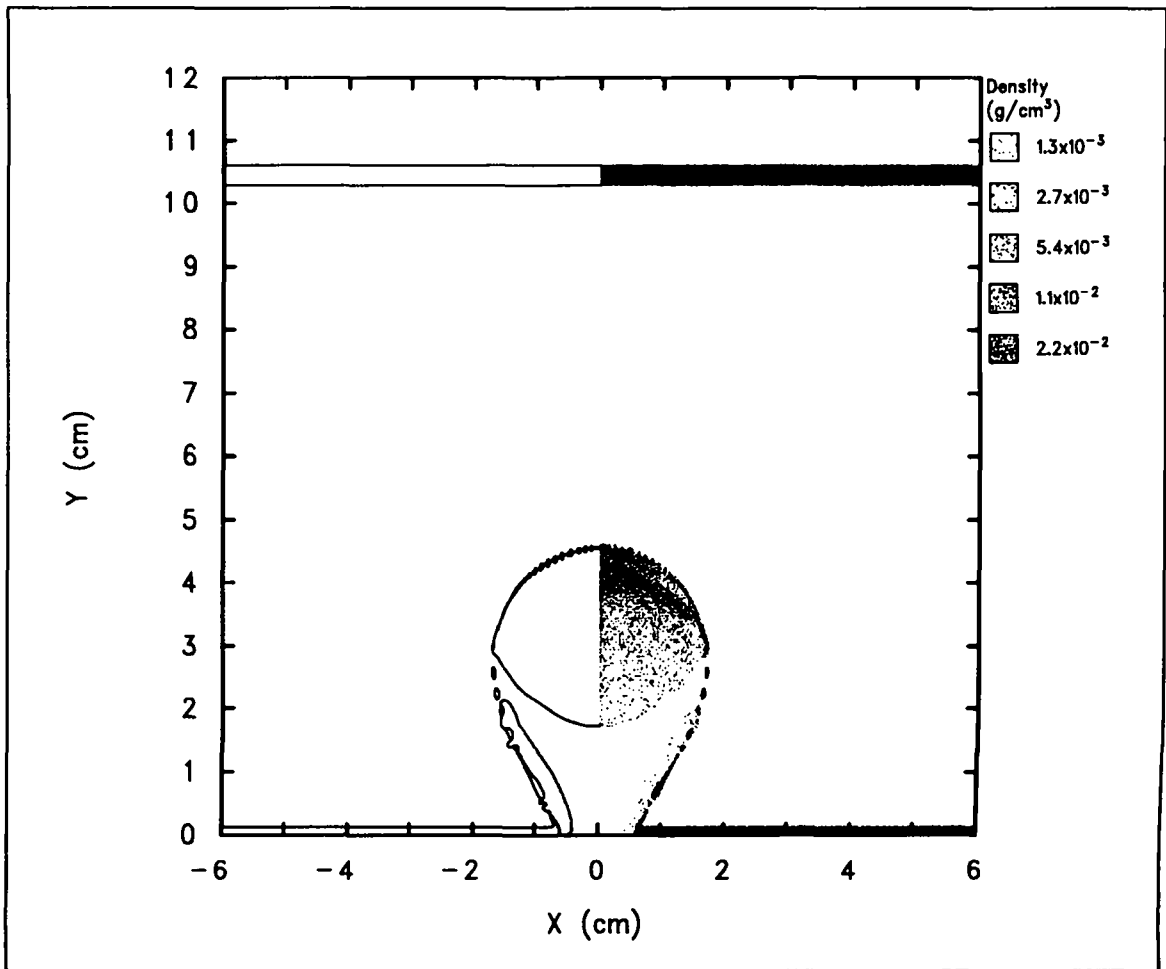


Figure 22. The na12-mcp CTH Simulation Halfway Between the Bumper and Rear Wall

Comparison of Analytic Whipple Bumper Shield Ballistic Limits with CTH Simulations

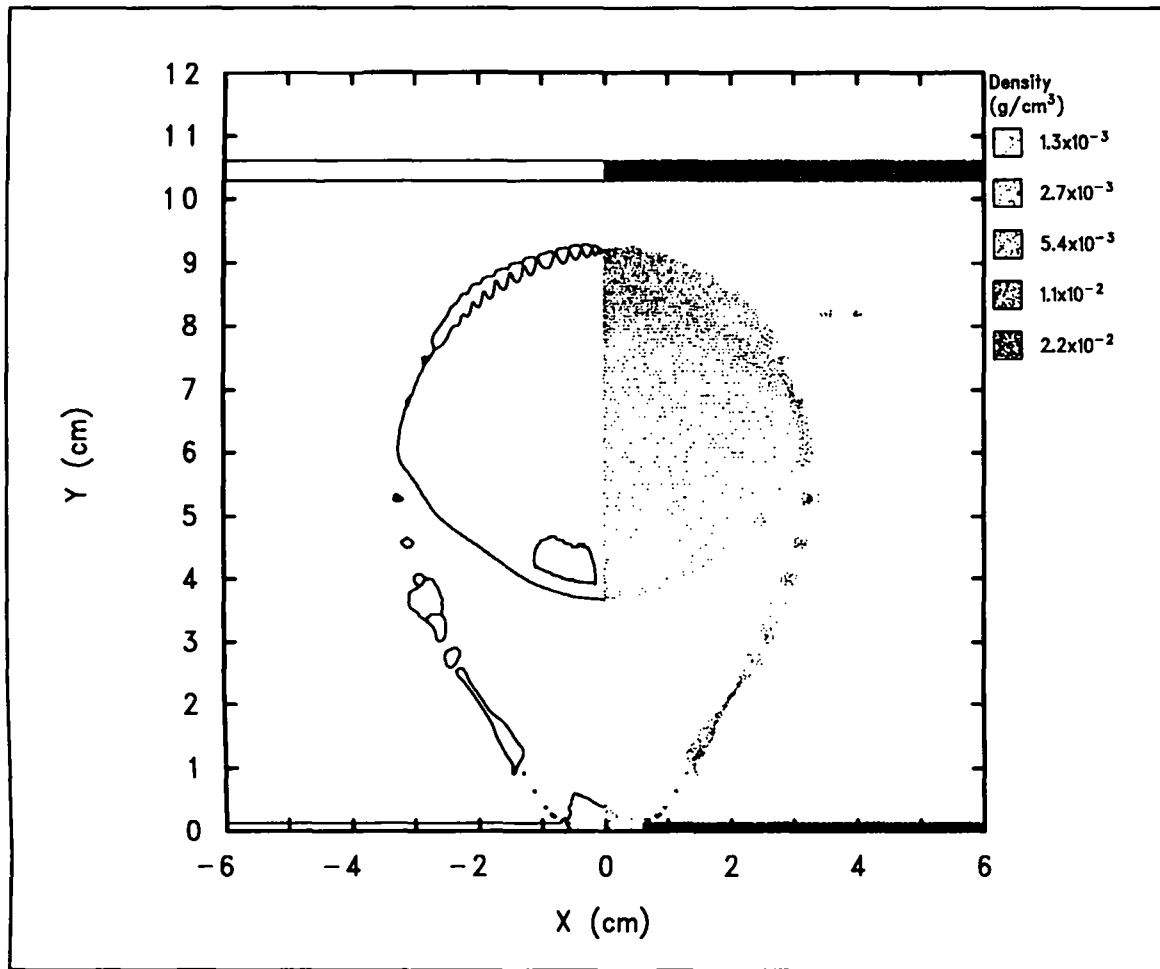


Figure 23. The na12-mcp CTH Simulation Just Before the Rear Wall

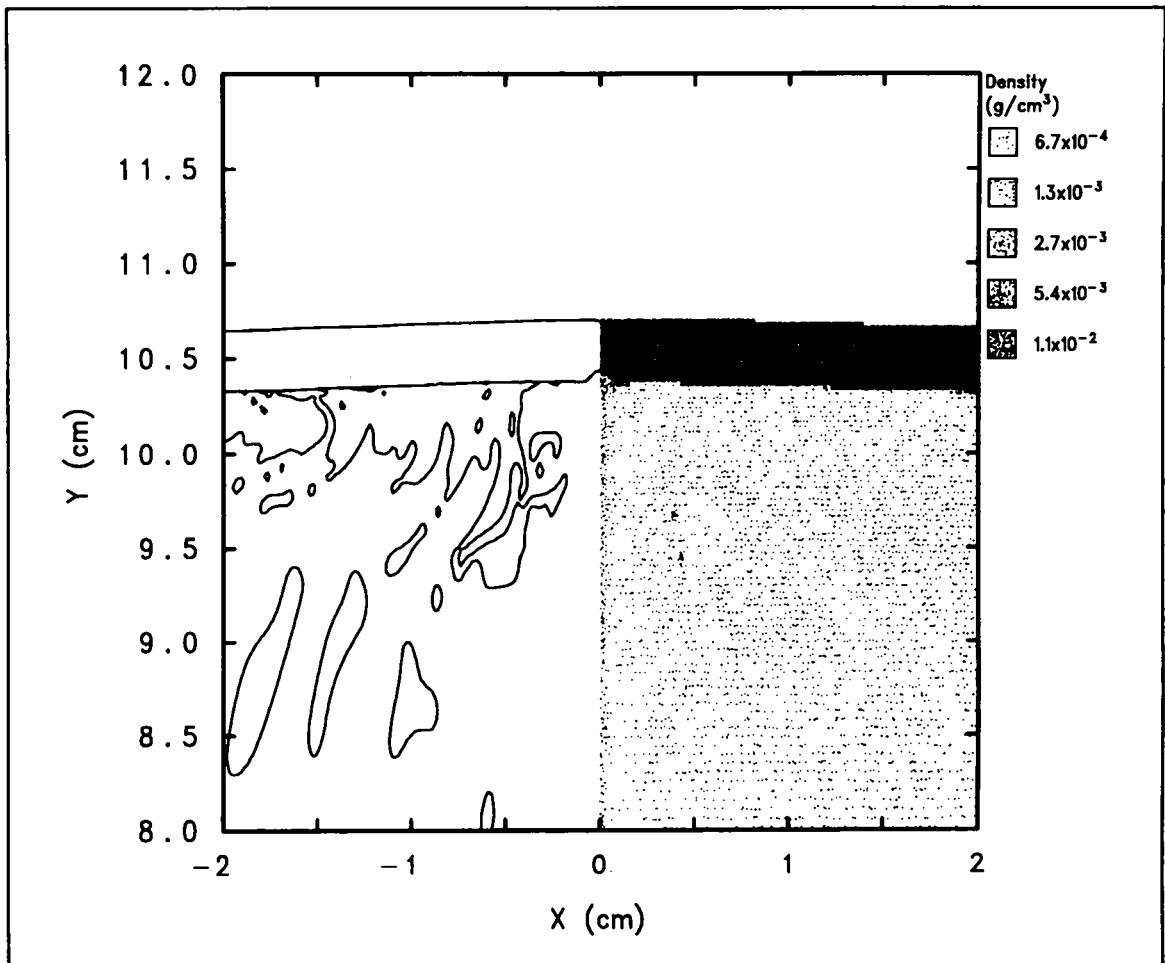


Figure 24. The na12-mcp CTH Simulation Rear Wall Terminal Damage

Oblique Impact

The next series of figures shows a representation of the debris cloud and the terminal rear wall damage for the single oblique CTH simulation. As noted in the previous section, the 3D simulation was completed using the rezoning feature of CTH to reduce the number of zones required. Figure 25 displays a linear-density representation of the debris cloud shortly ($2 \mu\text{s}$) after impact with the bumper shield. The linear-density along the line of sight, a computational representation of the same information available in a radiograph, is shown here as a “dot-density” plot. A 3D perspective view of the same information is provided in

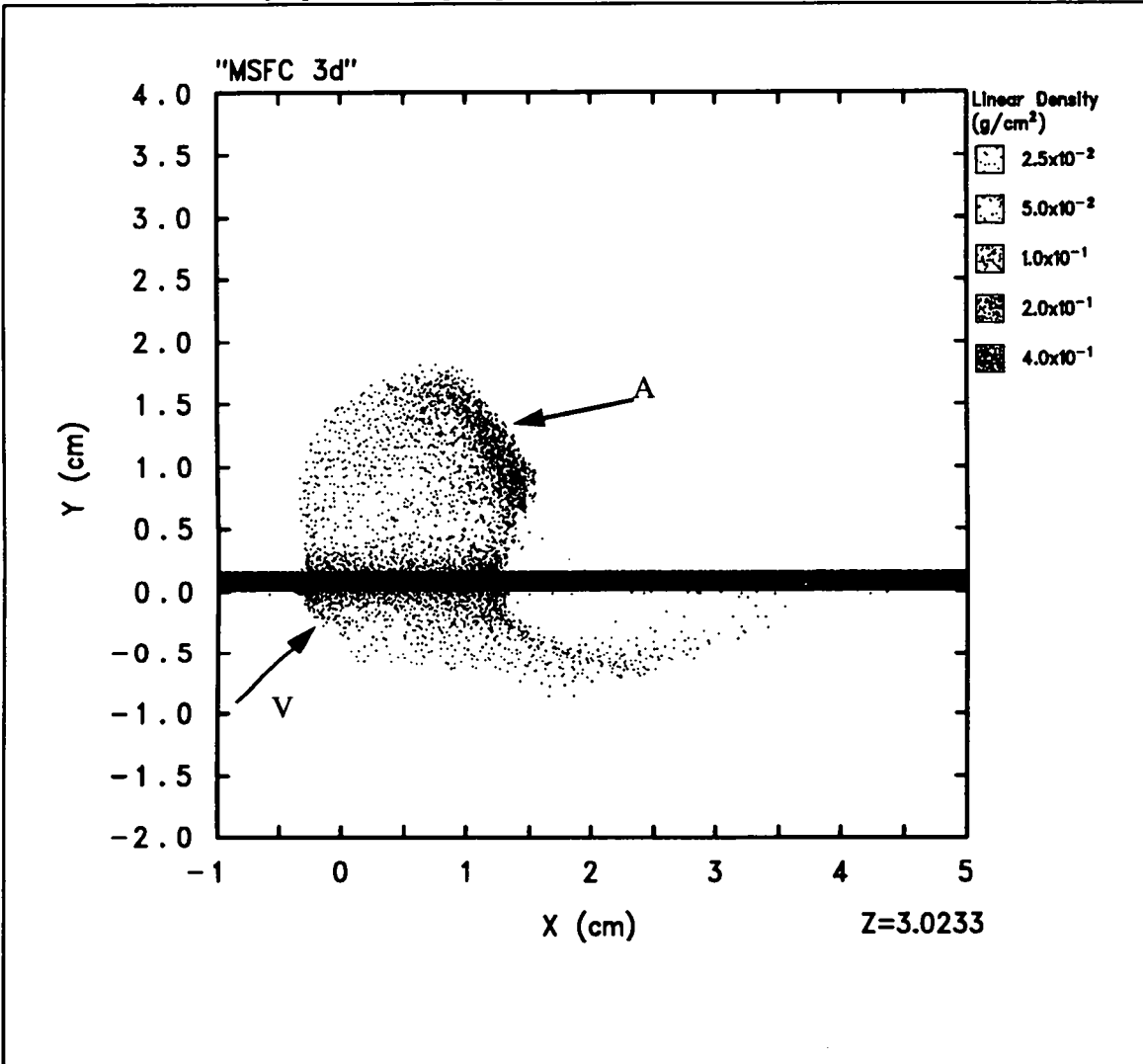


Figure 25. Computational Radiograph of CTH Simulation na12-ob at $2 \mu\text{s}$

Figure 26. An inspection of Figures 25 and 26 indicates that a substantial percentage of the mass of the projectile is ejected laterally and never perforates the bumper. Computational results also show that the debris cloud is composed of both bumper and projectile material with the highest density region consisting of predominately projectile material (location A in Figure 25).

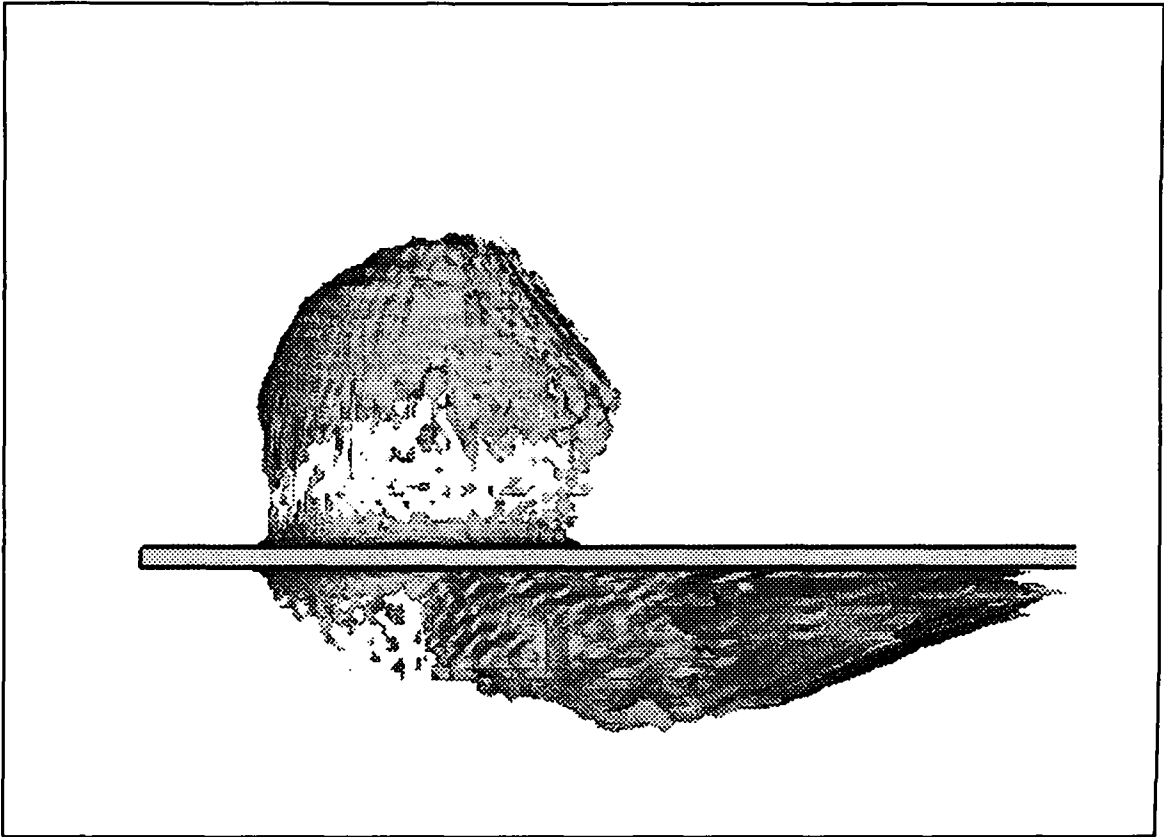


Figure 26. 3D Perspective View of CTH Simulation na12-ob at 2 μ s

Similar information is provided as the debris cloud approaches the rear wall in Figure 27. Again, the linear density is displayed as “dot-density” plot, the contour lines in Figure 27 are the material interfaces. The material interface lines represent that area in the cross-section where the volume fraction exceeds 0.5. This simulation was terminated at $\sim 21 \mu$ s. At this time, the majority of the debris cloud had impacted the rear wall and was rebounding back towards the bumper shield. Figure 28 displays a similar a 3D perspective view of the same information.

Figure 29 shows the terminal damage, as represented by the linear-density, to the rear wall. Very little deformation and or pitting is predicted by CTH for this particular impact. This is due to the relatively small amount of projectile mass that perforates the bumper.

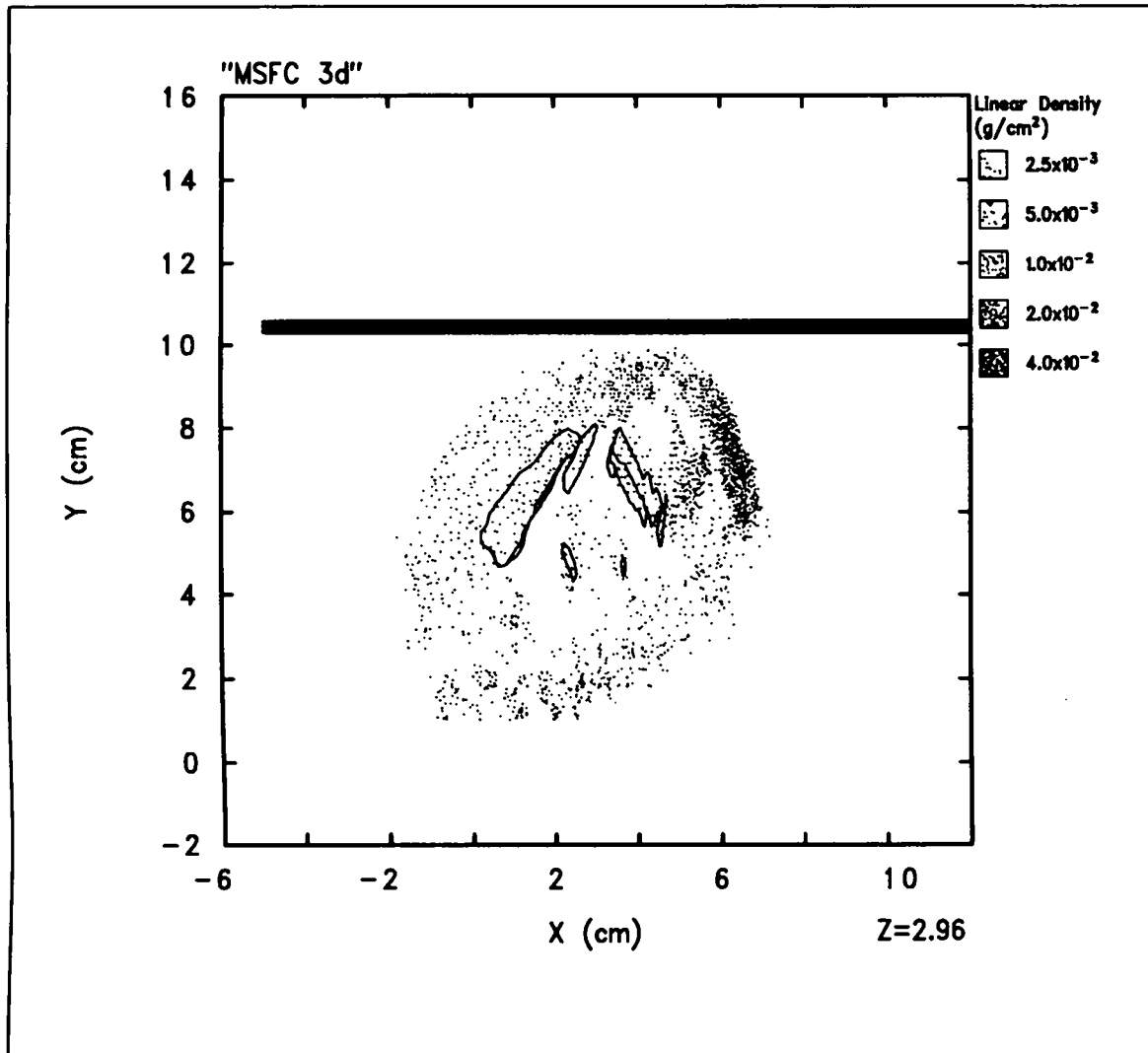


Figure 27. Computational Radiograph of CTH Simulation na12-ob at 11 μ s



Figure 28. 3D Perspective View of CTH Simulation na12-ob at 11 μ s

Comparison of Analytic Whipple Bumper Shield Ballistic Limits with CTH Simulations

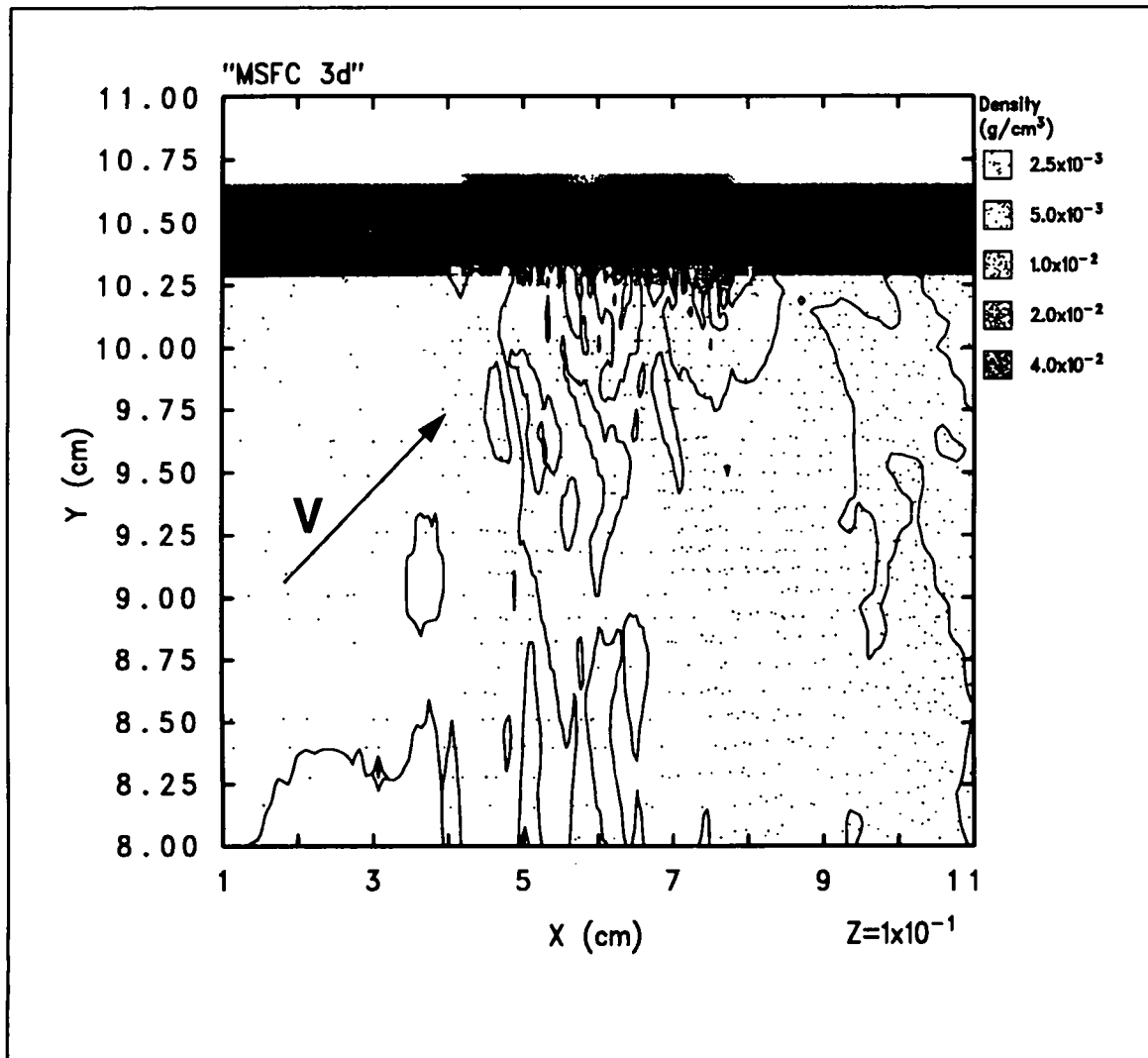


Figure 29. Terminal Rear Wall Damage for CTH Simulation na12-ob at 21 μs

Conclusions

The simulations described in this report were completed for two principal reasons. The first reason was to demonstrate the feasibility of completing 2 and 3D simulations of debris cloud formation and the subsequent loading on the rear wall by the debris cloud. The information contained in this report demonstrates that these simulations are feasible and can be completed in a reasonable amount of computer time. The average run time for the 6 axisymmetric simulations was ~3.5 hours time on a Cray YMP8/64. The single 3D simulation required ~45 hours time on a Cray YMP8/64. The ratio between the 2 and 3D run times is typical for problems of this magnitude.

The second reason for the simulations was to compare the analytic ballistic limits with the hydrocode results. Neither the analytic approximations nor the hydrocode models have been validated over the velocity range of 7 km/s to 12 km/s, primarily due to lack of experimental capabilities to launch the prerequisite size particles over that velocity range. So the comparison is between two (hydrocodes and analytic extrapolations) different techniques, neither of which has been extensively validated with experiment. However, the comparison is still interesting. Figure 30 shows the Wilkinson and Cour-Palais analytic curves over the 8 to 12 km/s velocity range with the CTH no-perforation/perforation locations noted by open circles and crosses, respectively. A very small number of CTH

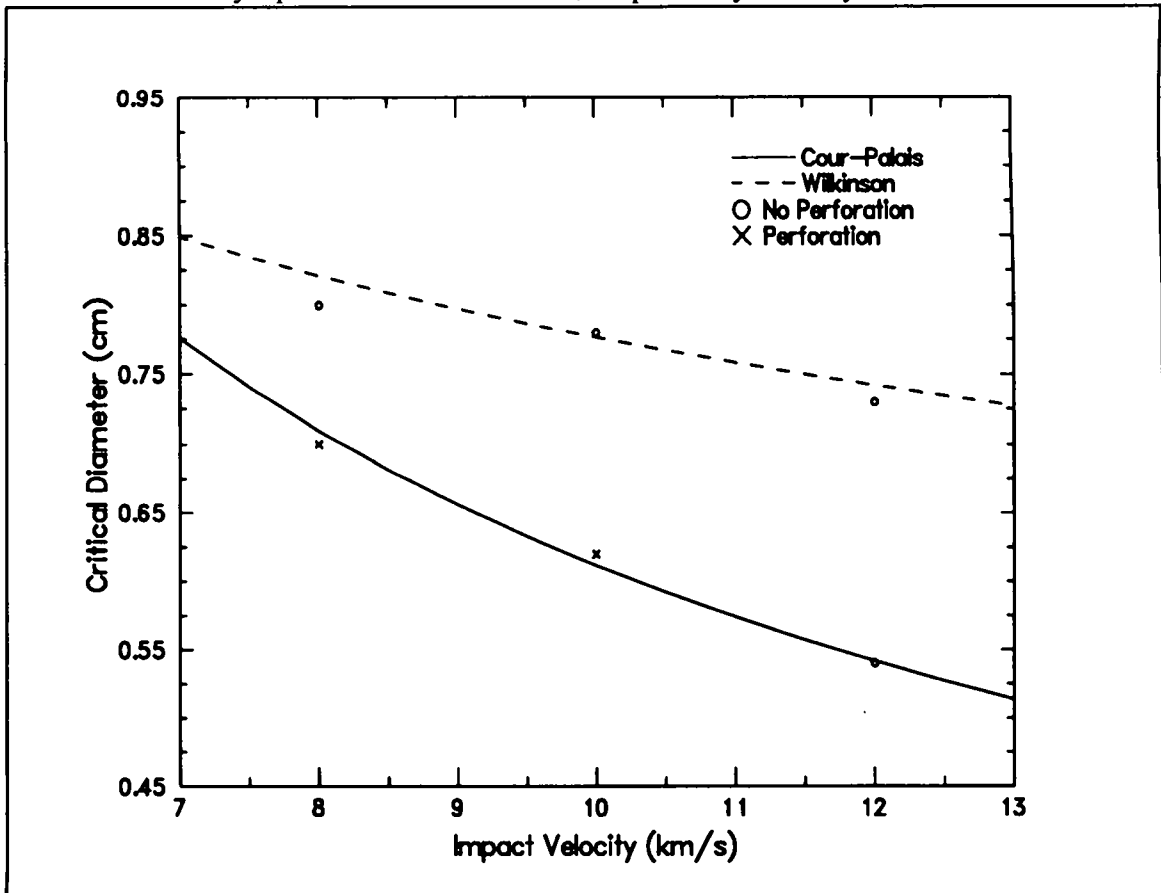


Figure 30. A Comparison of CTH and Analytic Ballistic Limits

Comparison of Analytic Whipple Bumper Shield Ballistic Limits with CTH Simulations

simulations were completed for this report and it is not possible to make an estimate of the sensitivity of the predictions on zone size, equations-of-state, strength models, or mesh refinement. Because of these limitations, no exact estimate of error can be placed on the CTH predictions. However, CTH has been shown^{14,15,16} to match experimental results to within ~10% on properly characterized simulations covering a wide range of phenomena.

Given the limited number of CTH points, the CTH determined ballistic limit lies between the two analytic estimates for velocities at or below 10 km/s. However, it appears that the CTH determined ballistic limit lies above both analytic estimates for velocities above 10 km/s. This may be due to the relatively short times considered in the CTH simulations. At high impact velocities, the loading on the rear wall is dominated by a time and space distributed impulse due to the high vapor content of the debris cloud. As the impact velocity increases, the amount of vapor increases (see Table 10). The loading produced by a debris cloud composed principally of vapor is significantly different than that of condensed phase matter. The damage produced in the rear wall is predominately bulging deformation. In addition, the rear wall is given a translational velocity. This later effect is due to inability to fix the edges of the computational rear wall. Even though there is no short time perforation due to the debris cloud impact, it is quite possible that a late time structural failure would occur due the bulge deformation. CTH will not model the late time structural failure due to time dependent loading.

At velocities below 8 km/s, CTH has been shown to correlate well with experiment¹⁷. Using a series of well characterized experiments, CTH was systematically compared to the experimental results. For a velocity range of 3 - 7 km/s, CTH predicted hole size in perforation events to within 10%. In addition, two data points exist for velocities near 10 km/s. CTH has been compared to the ~10 km/s impact experiments that were done at the Sandia HyperVelocity Launch Facility¹⁸. As for the lower velocity range, CTH has shown reasonable correlation with the experimental results near 10 km/s. Given the validation (although limited) of CTH for this class of impacts, the results noted in this report are indicative of potential trends in bumper shield phenomena. It is important to note that the analytic ballistic limit curves represent extrapolations from low velocity data and have not been validated above ~7 km/s.

The calculations described in this report demonstrate the feasibility of performing 2 and 3D simulations of orbital debris impacts on Whipple type shields. In addition, the correlation between analytic estimates of the ballistic limits of Whipple type shields and CTH estimates is reasonable given the experimental uncertainties of hypervelocity impacts on such shields.

References

- ¹L. C. Chhabildas, "An Impact Technique to Accelerate Flier-Plates to Velocities Over 12 km/s," in *The Proceeding of the Hypervelocity Impact Society - 1992*, to be published, 1992.
- ²L. C. Chhabildas, "A New Hypervelocity Launcher (HVL) for Space Science Applications," AIAA Paper No. 92-1639, *Proceedings of the AIAA Space Programs and Technologies Conference*, 1992.
- ³L. C. Chhabildas, L. M. Barker, J. R. Asay, T. G. Trucano, G. I. Kerley, and J. E. Dunn, *Launch Capabilities to Over 10 km/s, in Shock Waves in Condensed Matter - 1991*, Eds., S. C. Schmidt, J. W. Forbes, R. D. Dick, Elsevier Science Publishers B.V., 1992.
- ⁴J. P. D. Wilkinson, "A Penetration Criterion for Double-Walled Structures Subject to Meteoroid Impact," *AIAA Journal*, Vol. 7, pp. 1937-1943, 1969.
- ⁵B. G. Cour-Palais, "Meteoroid Protection by Multiwall Structures," AIAA Paper No. 69-372, *Proceedings of the AIAA Hypervelocity Impact Conference*, 1969.
- ⁶E. L. Christiansen, "Shield Sizing and Response Equations," NASA Johnson Space Center Technical Note SN3-91-42, 1991.
- ⁷E. S. Hertel, Jr., L. C. Chhabildas, S. A. Hill, "Whipple Bumper Shield Simulations," in *Shock Waves in Condensed Matter-1991*, edited by S. C. Schmidt, J. W. Jorbes, and R. D. Dick, Elsevier Science Publishers B. V., 1992.
- ⁸F. L. Whipple, "Meteoric Phenomena and Meteorites," in *Physics and Medicine of the Upper Atmosphere*, edited by C. S. White and O. O. Benson, Jr., University of New Mexico Press, Albuquerque, New Mexico, 1952.
- ⁹H. F. Swift, J. M. Carson, and A. K. Hopkins, "Ballistic Limits of 6061-T6 Aluminum Bumper Systems," Air Force Materials Laboratory Technical Report AFML-TR-68-257, September 1968.
- ¹⁰J. M. McGlaun, S. L. Thompson, L. N. Kmetyk, and M. G. Elrick, "A Brief Description of the Three-Dimensional Shock Wave Physics Code CTH," Sandia National Laboratories SAND89-0607, July 1990.
- ¹¹J. R. Asay, L. C. Chhabildas, G. I. Kerley, and T. G. Trucano, "High Pressure Strength of Shocked Aluminum," in *Shock Waves in Condensed Matter-1985*, edited by Y. M. Gupta, Plenum Publishers.
- ¹²D. R. Ek and J. R. Asay, "The Stress and Strain-Rate Dependence of Spall Strength in Two Aluminum Alloys," in *Shock Waves in Condensed Matter-1985*, edited by Y. M. Gupta, Plenum Publishers.
- ¹³G. I. Kerley, "Theoretical Equation of State for Aluminum," *Int. J. Impact Engng.*, Vol 5, pp. 441-449, 1987.

Comparison of Analytic Whipple Bumper Shield Ballistic Limits with CTH Simulations

- ¹⁴E. S. Hertel, Jr., "A Comparison of Calculated Results with Experimental Data for Long Rod Projectiles," Sandia National Laboratories SAND90-0610, December 1990.
- ¹⁵L. M. Kmetyk and P. Yarrington, "CTH Analyses of Explosively-Formed-Projectiles with Comparisons to Test Data," Sandia National Laboratories SAND89-2388, July 1990.
- ¹⁶L. M. Kmetyk and P. Yarrington, "Cavity Dimensions for High Velocity Penetration Events - A Comparison of Computational Results with Data," Sandia National Laboratories SAND88-2693, May 1989.
- ¹⁷E. S. Hertel, Jr. and L. Yarrington, "CTH Analyses of Orbital Debris Bumper Shield Test," Sandia National Laboratories report (to be published).
- ¹⁸L. C. Chhabildas and E. S. Hertel, Jr., "Determination of the Ballistic Limit for a Whipple Bumper Shield and Comparison with CTH Simulations," Sandia National Laboratories SAND92-0418, July 1992.

APPENDIX A

Sample CTH Input Deck for Axis-Symmetric Simulation

```
*eor*genin
*
MSFC Simulation na10-w 10km/s impact
*
control
ep
mmp
endcontrol
*
mesh
block 1 geom=2dc type=e

x0 0.0
x1 w=2.0 dxf=0.015 dxl=0.015
x3 w=7.0 dxf=-1.0 dxl=0.400
x4 w=5.0 dxf=-1.0 dxl=0.800
endx

y0 -1.0
y1 w=1.0 dyf=0.03 dyl=0.015
y2 w=1.0 dyf=-1.0 dyl=0.015
y3 w=5.0 dyf=-1.0 dyl=0.075
y4 w=5.0 dyf=-1.0 dyl=0.015
y5 w=3.0 dyf=-1.0 dyl=0.015
endy

xact = 0.0 0.5
yact = -0.5 0.0

endb
endmesh
*
```

```

insertion of material
block 1
  package 'aluminum sphere Al 1100-0'
  material 1
  numsub 50
  yvel 10.0e5
  insert circle
    center 0.0 -0.39
    radius 0.39
  endinsert
endpackage
package 'aluminum bumper Al 6061-T6'
  material 2
  numsub 10
  insert box
    x1 0.0 x2 10.0
    y1 0.0 y2 0.127
  endinsert
endpackage
package 'aluminum hull Al 2219-T87'
  material 3
  numsub 10
  insert box
    x1 0.0 x2 10.0
    y1 10.287 y2 10.6045
  endinsert
endpackage
endblock
endinsertion
*
eos
  mat1 sesame eos=205 feos='/usr/community/gkerley/b205'
  mat2 sesame eos=205 feos='/usr/community/gkerley/b205'
  mat3 sesame eos=205 feos='/usr/community/gkerley/b205' sr=0.947
endeos
*eor*cthin
*
MSFC Simulation na10-w 10km/s impact
*
control
  tstop = 25.0e-6
  cpshift = 600.0
  ntbad = 100000
endc
*
convct
  convection = 1
  interface = high
endc

```

```

*
edit
  shortt
    time = 0.0, dt = 1.0
  ends

  longt
    time = 0.0, dt = 1.0
  endl

  histt
    time = 0.0, dt = 1.0
  endh
*
plott
  time = 0.0, dt = 1.0e-6
endp
ende
*
epdata
  matep=1, yield=1.0e9, poisson=.333
  matep=2, yield=5.0e9, poisson=.333
  matep=3, yield=7.0e9, poisson=.333
  mix=3
ende
*
fracts
  stress
  pfrac1 -1.0e9
  pfrac2 -11.0e9
  pfrac3 -15.0e9
  pfmix -1.0e9
  pfvoid -1.0e6
endf
*
boundary
  bhydro
  block 1
    bxbot = 0 , bxtop = 1
    bybot = 2,, bytop = 2
  endb
endh
endb
*
mindt
  time = 0. dt = 1.e-12
endm
*

```

```
discard  
  mat 1 pressure 1.0e6 density -0.0001  
  mat 2 pressure 1.0e6 density -0.0001  
enddiscard
```

APPENDIX B

CTH Input Deck for Three-Dimensional Simulation

```
*eor*genin
*
3d spherical impactor at 45 degrees v=12.0 d=0.54
*
control
    usessd
    ep
    mmp
endcontrol
*
mesh
    block 1 geom=3dr type=e
    x0=-8.0
    x1 w=6.00 dx=0.350 dxl=0.100
    x2 w=1.60 dx=-1.0 dxl=0.030
    x3 w=0.80 dx=-1.0 dxl=0.030
    x4 w=1.60 dx=-1.0 dxl=0.100
    x5 w=6.00 dx=-1.0 dxl=0.350
    endx
    y0=-1.0
    y1 w=0.40 dy=0.070 dyl=0.055
    y2 w=0.60 dy=-1.0 dyl=0.031
    y3 w=0.124 dy=-1.0 dyl=0.031
    y4 w=5.076 dy=-1.0 dyl=0.250
    y5 w=5.087 dy=-1.0 dyl=0.040
    y6 w=0.64 dy=-1.0 dyl=0.040
    y7 w=2.00 dy=-1.0 dyl=0.100
    endy
    z0=0.0
    z1 w=0.42 dz=0.030 dzl=0.030
    z2 w=1.60 dz=-1.0 dzl=0.100
    z3 w=6.00 dz=-1.0 dzl=0.350
    endz
```

```
xact = -0.5,0.5  
yact = -0.6,0.2  
zact = 0.0,0.5
```

```
endb  
endmesh
```

```
insertion of material  
block 1  
package 'aluminum sphere Al 1100-0'  
  material 1  
  numsub 50  
  velocities xvel 8.48528e5  
  velocities yvel 8.48528e5  
  insert sphere  
    center 0.0, -0.27, 0.0  
    radius 0.27  
  endinsert  
endpackage  
package 'aluminum bumper Al 6061-T6'  
  material 2  
  numsub 10  
  insert cylinder  
    ce1 0.0, 0.000, 0.0  
    ce2 0.0, 0.127, 0.0  
    radius 12.0  
  endinsert  
endpackage  
package 'aluminum hull Al 2219-T87'  
  material 3  
  numsub 10  
  insert cylinder  
    ce1 0.0, 10.2870, 0.0  
    ce2 0.0, 10.6045, 0.0  
    radius 12.0  
  endinsert  
endpackage  
endblock  
endinsertion
```

```

eos
    mat1 sesame eos=105 feos='/usr/community/gkerley/b100'
    mat2 sesame eos=105 feos='/usr/community/gkerley/b100'
    mat3 sesame eos=105 feos='/usr/community/gkerley/b100' sr=0.947
endeos
*eor*cthin
*
* title record
*
3d spherical impactor at 45 degrees v=12.0 d=0.54
*
control
    usessd
    tstop = 12.0e-6
    cpshift = 600.
    ntbad = 100000
endc
*
convct
    convection = 1
    interface = high
endc
*
edit
    shortt
    tim = 0.0, dt = 1.0
    ends

    longt
    tim = 0.0, dt = 1.0
    endl
*
    plott
    tim = 0.0, dt = 1.0e-6
    endp
ende
*
epdata
    matep=1 , yield=3.0e8 , poisson=.333
    matep=2 , yield=3.0e9 , poisson=.333
    matep=3 , yield=5.0e9 , poisson=.333
    mix=1
ende

```

```

*
fracts
    stress
    pfrac1 -3.0e9
    pfrac2 -11.0e9
    pfrac3 -15.0e9
    pfmix -1.0e9
    pvoid -1.0e6
endf

boundary
    bhy
        bl 1
            bxb = 2 , bxt = 2
            byb = 2 , byt = 2
            bzb = 0 , bzt = 2
        endb
    endh
endb
*
mindt
    time = 0. dt = 1.e-12
endm
*
discard
    material 1 density=1.0e-4 pressure=1.0e6
    material 2 density=1.0e-4 pressure=1.0e6
    material 3 density=1.0e-4 pressure=1.0e6
    ton=25.0e-6
enddiscard

```


DISTRIBUTION:

Allahdadi, Firooz (3)
Phillips Laboratory
PL/WSSD
Kirtland AFB, NM 87117-6008
Attn: F. Allahdadi, D. Medina, & J.
Thomas

Anderson, Charles E. (5)
Southwest Research Institute
P.O. Drawer 28510
San Antonio, TX 78284
Attn.: C. E. Anderson, C. J. Kuhlman, D.
Littlefield, J. D. Walker, S. Mullin

Ari, Nasit (5)
Kaman Sciences Corporation
1500 Garden of the Gods Road
P. O. Box 7463
Colorado Springs, CO 80933
Attn: Nasit Ari, Tom Allen, Jeff Elder,
James Wilbreck, Sheldon Jones

Atkinson, Dale
POD Associates, Inc.
2309 Renard Place SE
Suite 201
Albuquerque, NM 87106

Beno, Joseph (3)
Defense Advanced Research Projects
Agency
3701 North Fairfax Drive
Arlington, VA 22203-1714
Attn: J. Beno, J. Richardson, R. Kocher

Bingham, Barry L.
Applied Research Associates
4300 San Mateo Blvd. NE
Suite A220
Albuquerque, NM 87110

Bradley, Kenneth R.
Defense Nuclear Agency
Washington, DC 20305-1000

Choo, Young-il(2)
Organization 81-12 - Bldg. 157
Lockheed Company
Sunnyvale, CA 94088-3504
Attn: Y. Choo & Eric Matheson

Clark, Dwight
Thiokol Corporation
Advanced Technology Division
P. O. Box 707
Mailstop 280
Brigham City, Utah 84302

Clark, Steve
MEVATEC
1525 Perimeter Parkway
Suite 500
Huntsville, AL 35806

Connell, John(2)
DNA/SPSP
6801 Telegraph Rd.
Alexandria, VA 22310
Attn: J. Connell & W. J. Tedeschi

Crawford, Richard
Logicon RDA
P. O. Box 92500
Los Angeles, CA 90009

Culp, Robert (2)
Department of Aerospace Engineering
Sciences
Campus Box 429
University of Colorado
Boulder, CO 80309
Attn: Robert Culp & Tim Maclay

Cykowski, Edward
Lockheed Engineering and Space
Company
Mail Code B22
2400 NASA Road 1
Houston, TX 77058-3711

Enig, Julius W.
Enig Associates, Inc.
11120 New Hampshire Ave.
Suite 500
Silver Spring, MD 20904-2633

Everhart, Doug
Battelle Memorial Institute
505 King Ave.
Columbus, OH 43201-2693

Fahrenthold, Eric P.
Department of Mechanical Engineering
The University of Texas
ETC 5.160
Austin, TX 78712

Flowers, John
LTV Missiles and Electronics Group
P. O. Box 650003
M/S EM-36
Dallas, TX 75265-0003

Fry, Mark
SAIC/New York
8 West 40th Street
14 Floor
New York, New York 10018

Gurule, Anthony
Orion International Inc.
Suite 200
300 San Mateo NE
Albuquerque, NM 87108

Hanson, Randy
Denver Research Institute
University of Denver
University Park
Denver, CO 80208

Havel, Thomas A.
U. S. Army Laboratory Command
Ballistic Research Laboratory
SLC BR-TR-AR
Aberdeen Proving Ground, MD 21005-
5066

Havens, Kenneth W.
LTV Missiles and Electronics Group
P. O. Box 650003
M/S EM-36
Dallas, TX 75265-0003

Herrick, Steven
Textron Defense Systems
Mail Stop 1115
201 Lowell St.
Wilmington, MA 01887

Holsapple, Keith A.
Department of Aeronautics and
Astronautics FS10
The University of Washington
FS10
Seattle, WA 98195

Hough, Gary
Aerophysics Research Facility
University of Alabama at Huntsville
Huntsville, AL 35899

Hunt, Ron(4)
Wright Laboratory
WL/MNSA
Eglin AFB, FL 32542-5434
Attn: J. Bailey, D. Brubaker, R. Hunt, and
B. Patterson

Johnson, Gordon R.
Alliant Techsystems Inc.
7225 Northland Dr.
Brooklyn Park, MN 55428

Kimsey, Kent (16)
U.S. Army Ballistic Research Laboratory
Attn.: SLCBR-TB-P
Aberdeen Proving Ground MD 21005-
5066
Attn: G. Bulmash, R. Coates, J. Dehn, Y.
Huang, K. Kimsey, H. Meyer, R. Mudd, J.
Petresky, G. Randers-Pehrson, D.
Scheffler, S. Segletes, G. Silsby, M. N.
Raftenberg, W. R. Somsy, B. Sorenson,
and M. Zoltuski

Louie, N. A.
Department Y831, Mail Station 13-3
McDonnell Douglas Missile Space
Systems Company
MDSSC
5301 Bolsa Avenue
Huntington Beach, CA 92647

Maewal, Akhilesh
Trans-Science Corporation
7777 Fay Avenue
Suite 112
La Jolla, CA 92037

Majerus, Mark
California Research and Technology, Inc.
PO Box 2229
Princeton, NJ 08543-2229

McDonald, James W.
General Research Corporation
Advanced Technologies Division
P. O. Box 6770
Santa Barbara, CA 93160-6770

Needham, Charles E.
Maxwell/S-CUBED
2501 Yale SE
Suite 300
Albuquerque, NM 87106

Orphal, Dennis L.(2)
California Research & Technology, Inc.
5117 Johnson Dr.
Pleasanton, CA 94588
Attn: D.L. Orphal & P. N. Schneidewind

Parnell, Kim T.
Failure Analysis Associates, Inc.
149 Commonwealth Ave.
P. O. Box 3015
Menlo Park, CA 94025

Pauley, Keith
PNL
KS-42
P. O. Box 999
Richland, WA 99352

Pierce, Ray
Physics International, Inc.
2700 Merced Street
San Leandro, CA 94577-0599

Radkowski, Peter P. F., III
Radkowski Associates, P. R. III
PO Box 1121
Los Alamos, NM 87544

Rau, Timothy
Physics International, Inc.
2700 Merced Street
San Leandro, CA 94577-0599

Salo, Glen (3)
BDM Corporation
1801 Randolph Road SE
Albuquerque, NM 87106
Attn: R. D. Mikatarian, D. W. Harmony,
and G. Salo

Singh, Bhuminder (4)
Teledyne Brown Engineering
300 Sparkman Drive
MS/50
P. O. Box 070007
Huntsville, AL 35807-7007
Attn: Brent Loper, Bhuminder Singh,
Marylin Wellman, Mitchell White

Smith, Mark
Aerophysics Branch
Calspan Corporation/AEDC Operations
MS 440
Arnold AFB, TN 37389

Spitale, Guy
Jet Propulsion Laboratory
California Institute of Technology
Reliability Engineering Section
4800 Oak Grove Drive
Pasadena, CA 91109

Tanner, William G., Jr.
Space Science Laboratory
Baylor University
PO Box 97303
Waco, TX 76798-7303

Webb, Brent
Umpqua Research Company
P. O. Box 791
125 Volunteer Way
Myrtle Creek, OR 97457

Weitz, Ronald L.
SAIC
2109 Air Park Road SE
Albuquerque, NM 87106

Wilbeck, James
Kaman Sciences Corporation
600 Boulevard South, Suite 208
P. O. Box 2486
Huntsville, AL 35804-2486

Dr. Michael Bjorkman
Boeing Defense and Space Group
JR-34
Huntsville, AL 35808

Eric Christiansen
NASA Johnson Space Center
Space Science Branch/SN3
Houston, TX 77058

Don Kessler
NASA Johnson Space Center
Space Science Branch/SN3
Houston, TX 77058

Ms. Jeanne Crews
SN3 - Hypervelocity Impact Laboratory
NASA, Johnson Space Center
Houston, TX 77058

NASA, Marshall Space Flight Center (10)
ED52 Structural Development Branch
Huntsville, AL 35812

Attention:
Ben Hayashida
Scott A. Hill (5)
Greg Olsen
Jennifer Robinson
Dr. Pedro Rodriguez
Joel Williamsen

The Boeing Co. (3)
P. O. Box 3999, Mail Stop 87-60
Seattle, WA 98124

Attention:
Mr. R. M. Schmidt
Dr. J. Shrader
Dr. E. Wilhelm

Lambert, Michael
European Space Agency
estec
P. O. Box 299
2200 AG Noordwijk
The Netherlands

McDonnell, JAM
Physics Laboratory
University of Kent at Canterbury
Kent CT2 7NR
United Kingdom

Cunningham, Tim
General Research Corporation
Advanced Technologies Division
P. O. Box 6770
Santa Barbara, CA 93160-6770

Jerome, David
AFATL/SAA
Eglin AFB, FL 32542-5434

Castleberry, Paul
DNA
6801 Telegraph Road
Alexandria, VA 22310-3398

Cour-Palais, Burt
McDonnell Douglas
Space System Division
Houston, TX 77062

Bloom, Bernard
Grumman Space Station Program Support
P. O. Box 4650
Reston, VA 22090

McKnight, Darren
Kaman Sciences Corporation
2560 Huntington Ave.
Suite 200
Alexandria, VA 22303

Nagel, Larry
Kaman Sciences Corporation
2560 Huntington Ave.
Suite 200
Alexandria, VA 22303

Isbell, William
General Research Corporation
Advanced Technologies Division
P. O. Box 6770
Santa Barbara, CA 93160-6770

Los Alamos National Laboratory
Mail Station 5000
P.O. Box 1663
Los Alamos, NM 87545

Attn: B. I. Bennett, MS B221
Attn: Chuck Wingate, MS
Attn: Bob Stellingwerf, MS
Attn: Tai Ho Tan, MS J970
Attn: J. W. Shaner, MS P915
Attn: S. P. Marsh, MS J970
Attn: T. Neal MS
Attn: J. Dienes, MS B216
Attn: J. N. Johnson MS B214
Attn: N. L. Johnson, MS B216
Attn: G. H. McCall, MS B218

University of California
Lawrence Livermore National Laboratory
7000 East Ave.
P.O. Box 808
Livermore, CA 94550

Attn: W. J. Nellis MS
Attn: N. Holmes MS
Attn: G. Pomykal MS

Sandia Internal:

0430 J. J. Bertin
1150 G. A. Samara
1153 R. A. Graham
1200 J. P. VanDevender
1201 M. J. Clauser
1400 E. H. Barsis
1431 J. M. McGlaun
1431 K. G. Budge
1431 M. G. Elrick
1431 E. S. Hertel (20)
1431 J. S. Peery
1431 S. J. Petney
1431 A. C. Robinson
1431 T. G. Trucano
1431 M. Wong
1432 P. Yarrington
1432 R. L. Bell
1432 P. J. Chen
1432 H. E. Fang
1432 A. V. Farnsworth
1432 G. I. Kerley
1432 M. E. Kipp
1432 F. R. Norwood
1432 S. A. Silling
1433 P. L. Stanton
1433 J. A. Ang
1433 M. Boslough
1433 L. C. Chhabildas (20)
1433 M. D. Furnish
1433 D. E. Grady
1433 C. H. Konrad
6312 L. Yarrington
7141 Technical Library (5)
7151 Technical Publications
7613-2 Document Processing
DOE/OSTI (10)
8523-2 Central Technical Files